NACA

RESEARCH MEMORANDUM

ROCKET-MODEL INVESTIGATION TO DETERMINE THE FORCE AND HINGE-MOMENT CHARACTERISTICS OF A HALF-DELTA TIP CONTROL ON A 59° SWEPTBACK DELTA WING BETWEEN MACH NUMBERS OF 0.55 AND 1.43

By C. William Martz, James D. Church, and John W. Goslee

Langley Aeronautical Laboratory
Langley Field, Va.

NATIONAL ADVISORY COMMITTEE
FOR AERONAUTICS

WASHINGTON

October 6, 1952

Classification cancelled or changed to Unclassified

By authority of NASA Tech Pub Announcement #103

(OFFICER AUTHORIZED TO CHANGE)

by 28 Aug 56

(GRADE OF OFFICER MAKING CHANGE)

5 Aug 56

DATE

NATIONAL ADVISORY COMMITTEE FOR AERONAUTICS

RESEARCH MEMORANDUM

ROCKET-MODEL INVESTIGATION TO DETERMINE THE FORCE AND HINGE-MOMENT CHARACTERISTICS OF A HALF-DELTA TIP CONTROL ON A 59° SWEPTBACK DELTA WING BETWEEN MACH NUMBERS OF 0.55 AND 1.43

By C. William Martz, James D. Church, and John W. Goslee

SUMMARY

A free-flight investigation of a rocket-powered control research model has been conducted to determine the force and hinge-moment characteristics of a half-delta tip control on a delta wing. The model consisted of a cylindrical body, with ogival nose and tail sections, equipped with a cruciform arrangement of 59° sweptback delta wings, the wing panels in one plane being equipped with half-delta tip controls.

Results show that the half-delta tip control could be so hinged that very small hinge-moment coefficients due to control deflection would be obtained at low angles of attack over the speed range tested. Although nonlinear variations of hinge moment with angle of attack were obtained with the control hinged at 63.9 percent control root chord, these moments were small over the speed range tested.

The center of pressure of the control-deflection forces at zero angle of attack had subsonic and supersonic locations of about 59 and $65\frac{1}{2}$ percent control root chord, respectively. The addition of $\pm 3^{\circ}$ angle of attack moved these locations forward from $1\frac{1}{2}$ to $2\frac{1}{2}$ percent root chord.

Over an angle-of-attack range of $\pm 4^{\circ}$, the center of pressure of the control angle-of-attack forces had a mean location of about 52 percent root chord at subsonic speeds and 58 to 61 percent root chord at supersonic speeds for zero control deflection.

Values of control normal force per unit deflection were roughly one-half as large as comparable values of control normal force per unit angle of attack. At supersonic speeds, 80 to 90 percent of the total

normal force developed by control deflection was carried on the control surfaces, the remaining 20 to 10 percent being induced on the model.

INTRODUCTION

Free-flight rocket tests (refs. 1 and 2) and wind-tunnel results (refs. 3 and 4) have indicated that half-delta wing-tip controls can provide satisfactory lateral control effectiveness in conjunction with relatively small hinge moments due to control deflection. In an effort to obtain more information about the effects of angle of attack on a control of this type (refs. 4 and 5), an investigation was made through the use of a rocket-powered model incorporating 59° sweptback delta wings with half-delta tip elevators.

Control hinge moments were obtained for two hinge-line locations at various combinations of angle of attack (from ±3° to ±11°) and control deflection (up to ±10°) between the Mach numbers of 0.55 and 1.43. By interpolating between the measured data, hinge-moment values were approximated for all combinations of angle of attack and control deflection within the test ranges. These moment data were used to determine the magnitude and chordwise location of control normal force as separate functions of angle of attack and control deflection.

Control lifting effectiveness data were also obtained for the complete configuration as were values of total lifting effectiveness.

The results are presented herein and compared with linear theory and other rocket-model data.

SYMBOLS

b	wing span, 2.58 feet
$\bar{c}$	wing mean aerodynamic chord, 1.46 feet
$\bar{c}_a$	control mean aerodynamic chord, 0.386 foot
c_a	control root chord, 0.579 foot
S	total wing area in one plane, 2.83 square feet
S_a	area of one control surface, 0.0964 square foot

δ	control surface deflection (positive deflection is trailing edge down), degrees
α	angle of attack, degrees
β	angle of sideslip, degrees
M	Mach number
ρ	mass density of air, slugs per cubic foot
V	free-stream velocity, feet per second
q	dynamic pressure, pounds per square foot, $\frac{\rho V^2}{2}$
μ	air-viscosity coefficient, slugs per foot-second
R	Reynolds number, $\frac{\rho \bar{c} V}{\mu}$
A_N	model normal acceleration, g units
g	acceleration of gravity, 32.2 feet per second squared
H	control hinge moment about hinge line, inch-pounds
C_h	control hinge-moment coefficient, $\frac{H/12}{qS_a\bar{c}_a}$
C_N	total normal-force coefficient, $\frac{\text{Normal force on model}}{qS}$
C_L	total lift-force coefficient, $\frac{\text{Lift force on model}}{qS}$
$(C_N)_a$	control normal-force coefficient, $\frac{\text{Normal force on control surface}}{qS_a}$
$(C_L)_a$	control lift-force coefficient, $\frac{\text{Lift on control surface}}{qS_a}$
$c.p._\delta$	chordwise center-of-pressure location of the control force due to control deflection (measured from control apex)
$c.p._\alpha$	chordwise center-of-pressure location of the control force due to angle of attack (measured from control apex)

$H_\delta = \frac{\partial H}{\partial \delta}$

$C_{h_\delta} = \frac{\partial C_h}{\partial \delta}$

$C_{h_\alpha} = \frac{\partial C_h}{\partial \alpha}$ (faired between $\alpha = -4$ and $\alpha = 4$ at $\delta = 0$)

$C_{N_\delta} = \frac{\partial C_N}{\partial \delta} \frac{S}{2S_a}$

$C_{N_\alpha} = \frac{\partial C_N}{\partial \alpha}$

$C_{L_\alpha} = \frac{\partial C_L}{\partial \alpha}$

$\left(C_{N_\delta}\right)_a = \frac{\partial (C_N)_a}{\partial \delta}$ at $\alpha = 0$

$\left(C_{N_\alpha}\right)_a = \frac{\partial (C_N)_a}{\partial \alpha}$ (faired between $\alpha = -4$ and $\alpha = 4$ at $\delta = 0$)

$\left(C_{L_\alpha}\right)_a = \frac{\partial (C_L)_a}{\partial \alpha}$

Subscripts:

1 refers to control with hinge line at $0.6390c_a$

2 refers to control with hinge line at $0.6885c_a$

MODEL

The hinge-moment research model used in this investigation consisted of a cylindrical body, with ogival nose and tail sections, equipped with a cruciform arrangement of 59° sweptback delta wings. A drawing of the model showing over-all dimensions is presented in figure 1 and photographs of the model are shown as figure 2.

The wing panels in one plane were equipped with 60° sweptback half-delta tip controls. The ratio of total control area to total exposed wing area in one plane (including control area) was 1/8.8. The wing panels had a modified hexagonal airfoil section of constant maximum thickness, the maximum thickness ratio of which varied from 2.37 percent at the root chord (fuselage center line) to 8.91 percent at the parting line of the wing and tip control. The tip controls, fastened to the outboard ends of torque rods, had modified double-wedge airfoil sections with a constant ratio of maximum thickness to chord of 3 percent. One control was hinged at 63.90 percent of its root chord and the other control was hinged at 68.85 percent of its root chord, the hinge line location remaining constant with respect to the wing in both cases. The controls were of solid steel construction and the parting line gap was 0.07 inch. Figure 3 shows the detail dimensions of the wing and tip control.

INSTRUMENTATION

The model was equipped with an NACA telemeter which transmitted the following flight data: normal, transverse, and longitudinal acceleration; static and total-pressure; deflection angle and hinge moments of each of two tip controls; and angle of attack.

A control-position indicator and balances to measure control hinge moments were constructed as integral parts of a power unit which was mounted in the rear part of the wing section of the model.

In addition to this model instrumentation, a radiosonde recorded atmospheric data at all flight altitudes shortly after the flight. Flight-path data were obtained with a radar tracking unit and CW Doppler radar was used to determine initial flight velocities. Photographic tracking was also employed to obtain visual records of the flight.

TECHNIQUE

The technique utilized in this investigation consisted of mechanically pulsing the controls as elevators throughout the flight so that their deflection varied sinusoidally with time. The response of the model to this sinusoidal control input involved a combination of sinusoidal pitching, rolling, and sideslip oscillations of the same frequency as the control input. The causes and effects of the rolling and sideslip oscillations will be discussed in the section on "Results and Discussion."

The control pulsing frequency was varied from 3.7 cycles per second at a Mach number of 1.46 to 1.5 cycles per second at a Mach number of 0.55 in an attempt to produce a nearly constant phase lag throughout the speed range between the model pitching response and the control input. The control pulsing amplitude varied from $\pm 8^{\circ}$ to $\pm 11^{\circ}$ because of varying deflection in the control linkage throughout the speed range. This technique allowed the continuous measurement of hinge moments for each of the controls at various combinations of control deflection and angle of attack over the Mach number range of the investigation.

From separate measurements of the variation of hinge moments with control deflection and angle of attack for each of the controls and a knowledge of the chordwise locations of the hinge lines, the chordwise location and magnitude of the control normal forces were determined as separate functions of angle of attack and control deflection. All hinge-moment data were corrected for inertia effects of the control and control linkage caused by the pulsing motion.

ACCURACY

The following information has been tabulated to illustrate possible errors in the basic measurements. These values are representative of the maximum instrument error in evaluating isolated data. In computations involving differences (such as slope determinations), possible errors in the component quantities can be considered roughly one-half as large as those shown below:

Quantity	Error
H_1, in.-lb	± 1.0
H_2, in.-lb	± 2.6
α, deg	± 0.52
δ, deg	± 0.40
A_N, g units	± 0.70
β, deg	± 0.6

RESULTS AND DISCUSSION

The variation of Reynolds number with Mach number is presented in figure 4. All data presented in this report were obtained during decelerated flight (from 0 to -3.5g).

Control Hinge Moments

As previously stated, hinge moments were measured on two control surfaces, the hinge-line locations of which were $0.6390c_a$ and $0.6885c_a$ (see fig. 3). Except for construction tolerances and hinge-line location, these controls were identical.

Since hinge moments were obtained at various combinations of control deflection and angle of attack, it was decided to present these data as a function of control deflection with various angles of attack indicated on the curves as shown in figure 5. These data are presented for both hinge-line locations and over a Mach number range of 0.55 to 1.43. Because it is usually more convenient to compare control hinge-moment data in coefficient form, a coefficient conversion factor has been included in each plot of figure 5. The irregularly shaped curves connecting the data points indicate the continuous hinge-moment information measured in this investigation. These curves are seen to be closed loops in some instances, and, in every case, to show at least one complete cycle of control-deflection and angle-of-attack information. Thus, at various angles of attack (within the angle-of-attack range at each Mach number), hinge moments were obtained at two different control deflections which are part of a hinge-moment-deflection curve at that angle of attack. Although the shape of this curve is not definitely known in all cases, it has been determined previously (ref. 2) that these curves at zero angle of attack are nearly straight lines (H_δ is constant with δ). It was decided, therefore, to assume that H_δ was constant with control deflection at all angles of attack investigated and to connect points of equal angle of attack with straight lines so as to obtain some indication of the separate effects of α and δ on control forces and hinge moments. It should be brought out at this point that, for the overlapping sections of some of the curves, there were three available test points through which the lines of constant α were faired and which generally constituted a straight line within the accuracy of the measurements. Since this method of straight-line fairing possibly could introduce considerable errors at the higher angles of attack, especially at the forward hinge line ($0.6390c_a$) where less linearity would be expected, the results obtained from this fairing should be considered mainly as trends. Regardless of the manner in which the constant α curves are faired, the important result is that all hinge moments presented are small over the speed range for the size of control tested. This is especially true for the control with the forward hinge-line location.

A complete set of data relating simultaneous values of angle of attack and control deflection at the various Mach numbers is presented in table I. This information is for both controls and is intended to supplement the angle-of-attack data presented in figure 5. Also included in table I are angles of sideslip which existed at the time the data were recorded — the sideslip resulting from coupling between the model rolling and pitching oscillations. [redacted]

Concerning the effects of sideslip, reference 6, which reports the theoretical aerodynamic properties of cruciform-wing and body combinations at subsonic, transonic, and supersonic speeds, concludes that lift and pitching moment are independent of the angle of sideslip. This conclusion would indicate, theoretically, that the hinge moments obtained in the present investigation were not affected by the sideslip. The effects of rolling depend upon the magnitude of the roll-induced helix angles. The maximum helix angle at the controls occurred at $M = 0.85$ and was of the order of 0.3°. This small angle would produce an incremental hinge moment of about one inch-pound, which is within the error of the hinge-moment measurements and, therefore, considered negligible.

Returning to figure 5, the reader will notice that considerable hinge-moment information is available from these plots. Hinge moments can be determined for all combinations of angle of attack and control deflection within the data loops at each Mach number by interpolation between the lines of constant angle of attack. Hinge moments also can be obtained in the region outside the data loops by reasonable extension of the constant angle-of-attack lines.

The parameters H_δ and C_{h_δ} are indicated by the slopes of the constant angle-of-attack curves for each of the hinge lines tested and for various angles of attack. Moreover, values of H_δ or C_{h_δ} can be determined for various other hinge-line locations by linear interpolation and extrapolation of the measured H_δ or C_{h_δ} values along the control chord. Negative H_δ or C_{h_δ} values indicate the control to be statically stable with deflection (i.e., the center of pressure of the deflection load is behind the hinge line) and positive values indicate the control to be statically unstable (center of pressure ahead of the hinge line). For the rearward hinge line ($0.6885c_a$), values of H_δ or C_{h_δ} are positive at all angles of attack and throughout the speed range. Similar values for the forward hinge line ($0.6390c_a$) are positive at all angles of attack for Mach numbers up to 0.90. Above the Mach number of 0.90, H_δ is seen to be negative at angles of attack near zero. As the angle of attack becomes larger, however, the center of pressure of the deflection force moves forward over the hinge line and H_δ becomes positive. The effect of H_δ becoming more positive as angle of attack is increased occurs for both hinge lines and over the Mach number range. This effect is apparent also from the results shown in figure 6 where values of C_{h_δ} are presented as a function of Mach number for each of the test hinge lines at angles of attack of 0° and -3°. Each of the curves is seen to be rather constant at subsonic and supersonic speeds with an abrupt negative shift as Mach number increases from 0.85 to 0.95. Values of C_{h_δ} are relatively small at all speeds for both hinge lines

and become more positive as angle of attack is increased from 0° to -3°. It should be pointed out, however, that the rate of change of C_{h_δ} with α decreased quite rapidly at the higher angles of attack for those Mach numbers where data were available.

The variation of hinge moments with angle of attack (fig. 5) can be seen for the rearward hinge line, to be fairly linear for control deflections near zero and somewhat less linear at the higher deflections. The data for the forward hinge line, however, show a definitely nonlinear variation with angle of attack at deflections other than zero and especially at supersonic speeds.

Values of the hinge-moment parameter C_{h_α} are presented in figure 7 as a function of Mach number for each of the two test hinge lines. These values represent faired slopes over an angle-of-attack range of ±4° and were obtained at zero control deflection. The curves are seen to have a similar variation with Mach number, with the larger subsonic values decreasing to small supersonic values. Values of C_{h_α} are positive over the speed range, thus indicating that the center of pressure of the control angle-of-attack loading remained forward of both test hinge lines. Actually, these center-of-pressure locations were determined from the assumed linear relationship between C_{h_α} and chordwise hinge-line location and will be presented later in the discussion.

The effect on C_{h_α} of increasing the angle of attack is indicated in figure 5 to be dependent upon the speed range. At Mach numbers less than 0.90 and deflections near zero, C_{h_α} tends to decrease with increasing angle of attack, while at supersonic speeds the reverse is observed.

At the higher deflections, C_{h_α} becomes larger when α and δ are both positive or both negative, whereas the values of C_{h_α} are smaller when α and δ are opposed. This is particularly true of the forward hinge-line results at supersonic speeds and is apparent from figure 8 which presents the variation of hinge moments with angle of attack for each of the test hinge lines at a Mach number of 1.43 for control deflections of -6°, 0°, and 6°. Also shown in figure 8 are the variations with α of the chordwise center-of-pressure location of the angle-of-attack loading for control deflections of -6°, 0°, and 6°. These curves were obtained from the above hinge-moment data. The center of pressure is seen to move forward with increasing angle of attack at

zero deflection. The relatively constant values of $c.p._{\alpha}$ when α and δ are of opposite sign and the large forward shift of $c.p._{\alpha}$ with increasing angle of attack when α and δ are of the same sign explains the previously mentioned variations of $C_{h_{\alpha}}$ at the higher deflections.

It should be noted that the variation of hinge moments with angle of attack for hinge-line locations other than those tested can be obtained by linear interpolation and extrapolation of the results presented in figure 5 along the control root chord.

For purposes of further analysis, the hinge-moment data were reduced to control-force data and are discussed in the following section.

Control Normal Force

The variations with Mach number of the control normal-force-coefficient slope and chordwise center-of-pressure location with respect to both angle of attack and control deflection are presented in figures 9 and 10 between the Mach numbers of 0.55 and 1.43. The normal-force-coefficient slope with deflection $\left(C_{N_{\delta}}\right)_a$ evaluated at $\alpha = 0$, is seen to vary smoothly over the Mach range with a maximum value of 0.05 at $M = 0.92$. This peak value is decreased about 30 percent at a Mach number of 1.4. Other rocket test data (ref. 2), shown for comparison, agree favorably with present test results. The effect of angle of attack on control normal-force magnitude is indicated by the slope of the normal-force-coefficient curve with angle of attack, which has been plotted against Mach number in figure 9. These values were obtained at $\delta = 0$ and represent a faired slope over the angle-of-attack range of $\pm 4^{\circ}$. Theoretical values of control-lift-curve slope (in coefficient form) were determined from reference 7 and are shown for comparison at supersonic speeds. The test curve is smooth and shows that values of $\left(C_{N_{\alpha}}\right)_a$ are roughly twice as large as comparable values of $\left(C_{N_{\delta}}\right)_a$. The theoretical curve, although considerably higher, has the same trend with Mach number as the experimental curve.

The variation with Mach number of the center of pressure of the control force resulting from control deflection ($c.p._{\delta}$) is shown in figure 10 for angles of attack of 0°, 3°, and -3°. The curve for zero angle of attack shows that the center of pressure has two principal locations over the speed range: a forward location of about 59 percent root chord for $M < 0.85$ and a rearward location of about $65\frac{1}{2}$ percent root chord for $M > 0.925$, with a linear transition between the Mach

numbers of 0.85 and 0.925. The supersonic values are from 1 to $1\frac{1}{2}$ percent forward of the linear theory prediction of 2/3 root chord. The curves for $\alpha = \pm 3^\circ$ are seen to have the same general shape as the $\alpha = 0$ curve, the important difference being the forward shift of $c.p._\delta$ due to the addition of α. The difference in the amount of shift between the curves at $\alpha = 3$ and at $\alpha = -3$ points out the asymmetry of the recorded data.

The chordwise location of the control normal force due to angle of attack ($c.p._\alpha$) is shown in figure 10 as a function of Mach number. As with its counterpart, $(C_{N_\alpha})_a$, this curve represents mean values over a $\pm 4^\circ$ angle-of-attack range at zero control deflection. At the lower subsonic speeds, $c.p._\alpha$ is seen to be constant at 52 percent root chord which corresponds to 28 percent mean aerodynamic chord. An abrupt 6 to $6\frac{1}{2}$ percent rearward shift in $c.p._\alpha$ occurs between the Mach numbers of 0.80 and 0.925. At supersonic speeds $c.p._\alpha$ varies from 58 percent at $M = 1$ to about $61\frac{1}{2}$ percent at $M = 1.4$, the latter value being identical to that predicted by linearized theory. It is now apparent that the Mach number variations of C_{h_α} (fig. 7) are due almost entirely to variations in $c.p._\alpha$. As stated before, $c.p._\alpha$ at control deflections near zero moves slightly rearward with increasing angles of attack for $M < 0.9$ and forward with increasing angles of attack at supersonic Mach numbers.

Total Normal Force

Figure 11 presents the variation of total normal force coefficient with control deflection at various angles of attack for $M = 1.3$. These results were obtained throughout the flight from normal accelerations and were corrected for the small effects of drag due to sideslip. The irregular curve represents the measured data and the lines of constant angle of attack are linear curves faired between end points of equal angle of attack. The slopes of the constant angle-of-attack lines are equal to C_{N_δ} and values of C_{N_α} can be obtained by cross-plotting the C_N intercepts of the faired curves at any control deflection.

It is apparent that the faired curves are nearly parallel and equally spaced along the C_N axis. The values of C_{N_δ} and C_{N_α} are independent, therefore, of angle of attack and control deflection, one value of each applying at all angles of attack and control deflections tested. Since the normal-force-coefficient plots at other Mach numbers

were similar, results are presented in the form of C_{N_α} and C_{N_δ}. These values are presented in figure 12 between the Mach numbers of 0.55 and 1.43. Unpublished experimental C_{L_α} results from a similar model are shown for comparison. The C_{N_α} values, although larger, compare favorably with the C_{L_α} values.

The C_{N_δ} curve, which represents the total normal force developed by control deflection at a fixed angle of attack, includes the normal forces induced on the model by control deflection (carry-over loading) as well as the loads carried directly on the control surface. Since the loads carried on the control have been determined independently from the hinge-moment data $\left((C_{N_\delta})_a\right.$, fig. 9$\left.\right)$, a measure of the control carry-over loading (in coefficient form) was obtained by subtracting $(C_{N_\delta})_a$ from C_{N_δ}. This carry-over loading is indicated in figure 12 by the ordinates of the shaded section between the curves. At supersonic speeds, the carry over is seen to be about 10 to 20 percent of the total load. These values are quite low as compared to linear theory predictions of 28 to 44 percent over the same Mach number range. At the lower Mach numbers, this percentage increases to a maximum of 45 at M = 0.8.

CONCLUSIONS

The following conclusions are drawn from the results of a rocket-model investigation between the Mach numbers of 0.55 and 1.43 of half-delta tip controls on a 59° sweptback delta wing with control hinge lines located at 63.9 and 68.85 percent control root chords:

1. Control hinge moments were relatively small throughout the speed range for all combinations of angle of attack and control deflections encountered during the test, particularly for the forward hinge-line location.

2. The center of pressure of the control-deflection loading at zero angle of attack had a subsonic location of about 59 percent control root chord and a supersonic location of about $65\frac{1}{2}$ percent root chord. The addition of ±3° angle of attack moved these locations forward $1\frac{1}{2}$ to $2\frac{1}{2}$ percent root chord.

3. The center of pressure of the control angle-of-attack loading ($c.p._\alpha$) had a mean location of about 52 percent root chord at subsonic

speeds and 58 to 61 percent root chord at supersonic speeds for zero control deflection. At supersonic speeds, c.p.$_\alpha$ moved forward with increasing angle of attack.

4. Values of control normal force per unit deflection were roughly one-half as large as comparable values of control normal force per unit angle of attack. At supersonic speeds, 80 to 90 percent of the total normal force developed by control deflection was carried on the control surfaces, the remaining 20 to 10 percent being induced on the model.

Langley Aeronautical Laboratory,
National Advisory Committee for Aeronautics,
Langley Field, Va.

[redacted]

REFERENCES

1. Sandahl, Carl A., and Strass, H. Kurt: Comparative Tests of the Rolling Effectiveness of Constant-Chord, Full-Delta, and Half-Delta Ailerons on Delta Wings at Transonic and Supersonic Speeds. NACA RM L9J26, 1949.

2. Martz, C. William, Church, James D., and Goslee, John W.: Free-Flight Investigation To Determine Force and Hinge-Moment Characteristics at Zero Angle of Attack of a 60° Sweptback Half-Delta Tip Control on a 60° Sweptback Delta Wing at Mach Numbers Between 0.68 and 1.44. NACA RM L51I14, 1951.

3. Scherrer, Richard, and Dennis, David H.: Lateral-Control Characteristics and Dihedral Effect of a Wing-Body Combination With a Variable-Incidence Triangular Wing and Wing-Tip Ailerons at a Mach Number of 1.52. NACA RM A50H10, 1951.

4. Conner, D. William, and May, Ellery B., Jr.: Control Effectiveness Load and Hinge-Moment Characteristics of a Tip Control Surface on a Delta Wing at a Mach Number of 1.9. NACA RM L9H05, 1949.

5. Jaquet, Byron M., Queijo, M. J., and Lichtenstein, Jacob H.: Low-Speed Static Longitudinal Stability and Control Characteristics of a 60° Triangular-Wing Model Having Half-Delta Tip Controls. NACA RM L51D20a, 1951.

6. Spreiter, John R.: Aerodynamic Properties of Cruciform-Wing and Body Combinations at Subsonic, Transonic, and Supersonic Speeds. NACA TN 1897, 1949.

7. Malvestuto, Frank S., Jr., Margolis, Kenneth, and Ribner, Herbert S.: Theoretical Lift and Damping in Roll at Supersonic Speeds of Thin Sweptback Tapered Wings With Streamwise Tips, Subsonic Leading Edges, and Supersonic Trailing Edges. NACA Rep. 970, 1950. (Supersedes NACA TN 1860.)

TABLE I.- TEST DATA

M = 0.55				M = 0.60				M = 0.70				M = 0.75				M = 0.80			
δ_1	δ_2	α	β	δ_1	δ_2	α	β	δ_1	δ_2	α	β	δ_1	δ_2	α	β	δ_1	δ_2	α	β
6.11	4.61		0.54	4.86	3.85		-3.98	- 4.98	-3.62		7.01	- 7.02	-5.78		5.30	9.88	8.03		-6.69
4.60	3.39		- .52	3.19	2.51		-4.64	- 2.86	-1.74		6.16	- 5.12	-4.11		5.74	9.96	8.02		-7.08
2.83	1.91	- 8.45	-1.79	1.46	1.10	-0.62	-5.22	- .54	.20	6.18	5.09	- 3.05	-2.28	2.63	5.98	9.56	7.87	-2.13	-7.11
1.06	.39	- 9.00	-3.18	- .30	- .29	- .32	-5.52	1.67	2.05	6.45	3.91	- .89	- .38	3.11	5.90	8.72	6.83	-2.77	-7.09
- 1.20	-1.37	- 9.15	-4.45	- 2.05	-1.70	.09	-5.59	3.94	3.85	6.47	2.58	1.27	1.49	3.40	5.61	7.52	5.94	-3.29	-6.88
- 3.28	-3.01	- 9.03	-5.46	- 3.87	-3.15	.51	-5.52	6.06	5.48	6.15	1.28	3.44	3.37	3.65	5.07	5.96	4.65	-3.78	-6.44
- 4.53	-3.99	- 8.58	-6.33	- 5.55	-4.51	.89	-5.10	7.97	6.90	5.47	.09	6.57	5.16	3.70	4.39	4.11	3.11	-4.28	-8.79
- 6.33	-5.39	- 7.96	-6.87	- 7.06	-5.72	1.30	-4.64	9.49	7.88	4.65	- .96	7.88	7.02	3.56	3.60	2.19	1.37	-4.64	-8.08
- 7.96	-6.68	- 7.13	-7.08	- 8.38	-6.80	1.62	-3.98	10.27	8.45	3.59	-2.30	8.98	7.86	3.29	2.71	.20	- .36	-4.91	-4.23
- 9.15	-7.66	- 6.09	-7.00	- 9.40	-7.64	2.04	-3.20	10.58	8.60	2.45	-3.58	9.98	8.58	2.83	1.66	- 1.82	-2.05	-5.04	-3.39
-10.18	-8.58	- 5.00	-6.65	-10.11	-8.20	2.32	-2.37	10.26	8.38	1.43	-4.80	10.47	8.90	2.18	.50	- 3.98	-3.87	-5.05	-2.38
-11.08	-9.17	- 3.57	-6.22	-10.52	-8.58	2.52	-1.47	9.76	7.89	.52	-5.87	10.49	8.78	1.64	- .49	- 6.06	-5.61	-4.82	-1.29
-11.11	-9.09	- 2.00	-5.57	-10.59	-8.56	2.85	- .44	8.88	7.11	- .41	-6.77	10:00	8.27	1.12	-1.26	- 7.90	-7.11	-4.42	- .21
-10.95	-8.93	- .50	-4.90	-10.52	-8.49	3.02	.21	7.63	6.06	-1.10	-7.40	9.12	7.47	.60	-2.58	- 9.47	-8.36	-3.81	.64
-10.57	-8.52	1.22	-4.15	- 9.93	-8.03	3.24	1.06	5.98	4.70	-1.68	-7.75	7.91	6.46	.15	-3.78	-10.74	-9.48	-3.05	1.67
- 9.97	-8.04	3.01	-3.28	- 9.18	-7.33	3.26	1.91	4.05	3.13	-2.24	-7.80	6.50	5.23	- .26	-4.84	-11.46	-9.92	-2.21	2.88
- 9.16	-7.31	4.63	-2.40	- 7.98	-6.37	3.44	2.64	1.98	1.42	-2.68	-7.47	4.85	3.87	- .39	-5.59	-11.38	-9.88	-1.23	4.00
- 8.09	-6.39	6.20	-1.53	- 6.63	-5.27	3.45	3.40	- .10	- .29	-2.97	-6.77	3.17	2.46	- .57	-6.19	-11.23	-9.63	- .20	5.18
- 6.90	-5.27	7.69	- .63	- 5.02	-3.96	3.51	3.93	- 2.43	-2.21	-3.24	-5.75	1.66	1.25	- .55	-6.53	-10.80	-9.13	.93	6.02
- 5.40	-3.97	9.16	.13	- 3.28	-2.55	3.51	4.46	- 4.63	-4.05	-3.36	-4.48	- .14	- .23	- .52	-6.54	-10.13	-8.39	1.96	6.71
- 3.80	-8.61	10.20	.89	- 1.52	-1.11	3.51	4.76	- 6.88	-5.76	-3.35	-3.18	- 1.82	-1.59	- .43	-6.26	- 9.14	-7.38	3.06	7.14
- 1.91	-1.02	11.10	1.77	.45	.50	3.21	4.92	- 8.67	-7.33	-3.18	-1.72	- 3.57	-3.00	- .32	-5.70	- 7.94	-6.07	4.07	7.38
.03	.50	11.28	2.66	2.25	1.97	2.88	4.97	-10.10	-8.53	-2.83	.22	- 5.29	-4.40	- .29	-4.95	- 6.49	-4.65	4.97	7.38
1.97	1.87	11.37	3.37	4.03	3.40	2.57	4.85	-11.09	-9.23	-2.39	.88	- 6.85	-5.69	- .18	-3.86	- 4.50	-2.76	5.85	7.06
3.64	3.31	11.34	4.06	5.74	4.77	2.00	4.58	-11.31	-9.67	-1.61	2.35	- 8.20	-6.83	- .08	-2.75	- 2.59	-1.08	6.38	6.48
5.44	4.86	10.77	4.69	7.26	5.97	1.50	4.09	-11.34	-9.65	- .91	3.67	- 9.24	-7.75	.06	-1.54	- .44	.68	6.79	5.71
7.10	6.28	9.81	5.14	8.40	6.86	.92	3.54	-10.95	-9.25	- .27	4.99	-10.16	-8.50	.16	- .28	1.70	2.43	6.98	4.75
8.45	7.34	8.78	5.44	9.27	7.55	.38	2.76	-10.10	-8.46	.73	6.09	-10.78	-9.02	.37	.50	3.83	4.14	6.97	3.64
9.43	8.11	7.17	5.57	9.82	7.99	- .02	1.98	- 8.98	-7.42	1.68	6.93	-11.03	-9.21	.58	1.76	5.92	5.87	6.53	2.52
10.16	8.72	5.65	5.51	9.87	7.97	- .55	1.15	- 7.68	-6.22	2.51	7.28	-11.09	-9.23	.94	2.92	7.80	7.29	5.92	1.89
10.48	8.86	3.73	5.34	9.78	7.86	- .97	.25	- 5.91	-4.62	3.36	7.37	-10.78	-8.95	1.27	3.77	9.46	8.40	5.02	.13
10.35	8.57	1.82	4.88	9.17	7.35	-1.30	- .55	- 4.04	-2.94	4.25	7.04	-10.17	-8.43	1.70	4.53	10.39	8.87	3.95	- .69
9.92	8.11	- .19	4.30	8.28	6.61	-1.39	-1.40	- 1.88	-1.08	4.85	6.35	- 9.41	-7.71	2.16	5.11	10.95	9.00	2.97	-2.00
9.26	7.40	- 3.01	3.48	7.11	5.66	-1.86	-2.44	.43	.88	5.30	5.53	- 7.89	-6.40	2.61	5.38	10.88	8.98	1.92	-3.35
8.37	6.51	- 3.77	2.33	5.60	4.43	-1.53	-3.71	2.56	2.66	5.63	4.41	- 7.22	-5.74	3.00	5.45	10.20	8.43	.83	-4.46
7.27	5.57	- 5.36	1.19	3.98	3.08	-1.42	-3.24	4.63	4.36		3.22	- 5.85	-4.49		5.28	9.77	7.90	- .02	-5.49
5.79	4.36	- 6.76	.04	2.26	1.70	-1.11	-4.74	5.75	6.03		2.00	- 4.25	-3.13		4.94	8.64	6.93	- .91	-6.49
4.22	3.07	- 7.66	-1.17	.61	.42	- .84	-5.22									7.39	5.75		-7.33
2.59	1.73	- 8.33	-2.66	- 1.23	-1.06	- .37	-5.47									5.81	4.50		-7.92
.67	.16		-3.95	- 3.01	-2.48		-5.56												
- 1.23	-1.40		-5.08	- 4.67	-3.81		-5.40												

TABLE I.- TEST DATA - Continued

M = 0.85				M = 0.90				M = 0.95				M = 1.00			
δ_1	δ_2	α	β	δ_1	δ_2	α	β	δ_1	δ_2	α	β	δ_1	δ_2	α	β
7.24	6.26		-0.78	- 5.20	-3.44		5.23	8.68	7.03		-4.62	- 9.84	-8.16		5.18
8.13	6.78		-1.37	- 3.48	-1.81		4.38	9.04	7.28		-4.52	-10.14	-8.11		5.04
8.76	7.10	-0.93	-1.80	- 1.46	- .12	6.04	3.42	9.08	7.22	-4.01	-4.24	-10.18	-7.81	4.09	4.73
9.20	7.26	-2.89	-2.25	.56	1.49	6.04	2.31	8.92	6.88	-4.70	-3.84	- 9.81	-7.29	4.88	4.20
9.43	7.32	-4.44	-2.49	2.47	3.03	5.78	1.14	8.29	6.14	-5.20	-3.38	- 9.09	-6.83	5.47	3.50
9.47	7.24	-5.81	-2.64	4.14	4.28	5.30	.14	7.23	5.04	-5.35	-2.83	- 8.21	-5.76	5.88	2.66
9.28	6.95	-7.01	-2.83	5.83	5.58	4.63	- .85	5.65	3.77	-5.62	-2.16	- 6.91	-4.65	6.04	1.73
8.81	6.47	-8.02	-2.94	7.23	6.60	3.81	-1.93	4.00	2.29	-5.58	-1.50	- 5.26	-3.22	5.95	.75
8.03	5.69	-8.64	-2.96	8.39	7.40	2.77	-2.86	1.95	.56	-5.25	- .81	- 3.39	-1.73	5.67	- .09
6.89	4.69	-9.03	-2.91	9.17	7.93	1.75	-3.81	0	-1.00	-4.74	- .08	- 1.32	- .26	5.09	- .90
5.62	3.56	-9.07	-2.77	9.60	8.12	.77	-4.58	- 2.01	-2.65	-4.03	.65	.59	1.15	4.23	-1.77
3.98	2.21	-8.85	-2.58	9.68	8.06	- .30	-5.20	- 3.86	-4.08	-3.24	1.55	2.23	2.36	3.35	-2.58
2.21	.77	-8.22	-2.26	9.50	7.73	-1.25	-5.67	- 5.52	-5.40	-2.43	2.35	3.72	3.42	2.36	-3.30
.41	- .64	-7.34	-1.73	8.85	7.07	-2.11	-5.96	- 7.02	-6.57	-1.52	3.21	5.13	4.41	1.22	-3.72
- 1.16	-1.87	-6.15	-1.07	7.88	6.07	-2.91	-6.09	- 8.14	-7.37	- .53	3.96	6.48	5.39	.15	-4.07
- 2.90	-3.17	-4.73	- .55	6.32	4.66	-3.55	-6.05	- 9.09	-8.04	.36	4.64	7.46	6.06	-1.01	-4.22
- 4.39	-4.32	-3.14	.04	4.48	3.12	-4.06	-5.86	- 9.70	-8.35	1.32	5.16	8.26	6.64	-2.11	-4.20
- 5.65	-5.16	-1.48	.51	2.77	1.59	-4.39	-5.55	-10.04	-8.40	2.25	5.47	8.89	7.04	-3.02	-4.07
- 6.85	-5.88	.28	1.04	.91	- .05	-4.82	-5.08	-10.13	-8.22	3.14	5.52	9.03	7.22	-3.86	-3.76
- 7.78	-6.37	1.89	1.73	- .95	-1.64	-4.76	-4.49	- 9.86	-7.70	4.05	5.32	9.14	7.14	-4.63	-3.40
- 8.66	-6.81	3.85	2.26	- 2.88	-3.26	-4.69	-3.78	- 9.19	-6.91	4.77	4.84	9.00	6.74	-5.26	-2.87
- 9.52	-7.12	5.26	2.84	- 4.64	-4.70	-4.52	-2.94	- 8.14	-5.85	5.45	4.21	8.43	6.14	-5.56	-2.47
-10.11	-7.38	6.86	3.16	- 6.50	-6.22	-4.18	-1.88	- 6.86	-4.68	5.88	3.42	7.43	5.25	-5.83	-1.93
-10.65	-7.68	8.23	3.45	- 8.04	-7.45	-3.66	- .81	- 5.21	-3.26	6.12	2.45	5.99	3.99	-5.84	-1.39
-10.87	-7.76	9.27	3.68	- 9.22	-8.40	-3.01	.16	- 3.22	-1.57	6.09	1.37	4.37	2.56	-5.75	- .82
-10.74	-7.57	10.01	3.61	- 9.96	-8.99	-2.31	1.10	- 1.17	- .05	5.89	.36	2.51	.98	-5.39	- .31
-10.29	-7.16	10.48	3.53	-10.41	-9.31	-1.51	2.21	.78	1.52	5.33	- .59	.62	- .52	-4.83	.26
- 9.46	-6.50	10.61	3.20	-10.63	-9.38	- .58	3.23	2.58	2.86	4.48	-1.50	- 1.16	-1.95	-4.14	.90
- 8.36	-5.62	10.53	2.76	-10.66	-9.21	.35	4.13	4.41	4.16	3.60	-2.35	- 2.94	-3.36	-3.29	1.53
- 7.09	-4.60	10.13	2.26	-10.32	-8.73	1.42	4.97	6.07	5.38	2.55	-3.16	- 4.51	-4.53	-2.54	2.25
- 5.58	-3.34	9.21	1.58	- 9.78	-8.07	2.29	5.59	7.38	6.29	1.24	-3.80	- 5.97	-6.56	-1.66	2.96
- 3.70	-1.97	8.06	.86	- 8.82	-6.97	3.25	5.92	8.33	6.94	.07	-4.30	- 7.18	-5.69	- .70	3.61
- 1.82	- .65	6.66	.38	- 7.51	-5.63	4.06	6.16	8.89	7.32	-1.21	-4.60	- 8.17	-7.27	.20	4.17
- .13	.50	5.08	- .11	- 5.86	-4.03	4.92	6.05	9.20	7.47	-2.21	-4.68	- 8.98	-7.79	1.15	4.61
1.33	1.45	3.52	- .45	- 3.98	-2.27	5.49	5.82	9.07	7.25	-3.29	-4.63	- 9.63	-8.11	2.06	4.82
2.62	2.29	1.81	- .90	- 2.03	- .57	5.87	5.33	8.67	6.82	-3.99	-4.41	- 9.98	-8.15	3.02	4.86
3.91	3.14	.05	-1.29	- .06	1.06	6.10	4.75	7.99	6.03	-4.66	-4.11	-10.17	-7.99		4.72
5.02	3.90	-1.49	-1.65	1.88	2.70	6.08	3.94	6.79	4.90	-5.16	-3.73	- 9.91	-7.42		4.36
6.18	4.72		-1.97	3.86	4.23		2.98	5.19	3.54		-3.25				
7.26	5.51		-2.20	5.77	5.66		1.90	3.27	1.86		-2.68				

NACA

TABLE I.- TEST DATA - Concluded

M = 1.10				M = 1.20				M = 1.30				M = 1.43			
δ_1	δ_2	α	β	δ_1	δ_2	α	β	δ_1	δ_2	α	β	δ_1	δ_2	α	β
- 9.41	-7.14		4.16	- 8.14	-5.81		3.49	- 1.58	-0.02		0.87	9.42	8.09		-1.93
- 8.43	-6.12		3.65	- 6.88	-4.60		2.71	.37	1.82		.05	9.43	7.84		-2.14
- 7.29	-5.01	4.73	2.97	- 5.10	-2.84	4.87	1.87	2.20	2.93	3.46	- .80	8.99	7.23	-3.50	-2.24
- 5.75	-3.47	4.98	2.16	- 3.17	-1.31	4.79	.90	3.91	4.19	2.74	-1.58	8.24	6.38	-3.90	-2.31
- 3.84	-1.79	5.06	1.28	- 1.13	.16	4.55	.04	5.62	5.39	1.85	-2.26	6.97	5.15	-4.18	-2.30
- 1.77	- .36	4.94	.39	.72	1.59	3.96	- .90	6.90	6.36	.86	-2.85	5.30	3.59	-4.20	-2.28
.01	1.02	4.60	- .43	2.46	2.87	3.26	-1.71	8.00	7.16	- .17	-3.26	3.29	1.84	-4.19	-2.02
1.86	2.41	3.99	-1.34	4.15	4.10	2.31	-2.48	8.77	7.66	-1.10	-3.50	1.43	.27	-4.01	-1.72
3.60	3.68	3.15	-2.13	5.61	5.09	1.32	-3.09	9.24	7.89	-1.97	-3.61	- .20	-1.16	-3.64	-1.36
5.26	4.82	2.23	-2.84	6.82	6.01	.31	-3.49	9.38	7.69	-2.86	-3.60	- 1.80	-2.51	-3.14	- .87
6.54	5.77	1.27	-3.40	7.88	6.76	- .81	-3.73	8.87	7.13	-3.58	-3.50	- 3.47	-3.93	-2.59	- .33
7.60	6.54	.27	-3.81	8.69	7.31	-1.77	-3.77	8.08	6.17	-4.29	-3.28	- 4.97	-5.18	-1.94	.30
8.38	7.09	- .67	-4.04	9.14	7.50	-2.80	-3.65	6.96	4.97	-4.73	-2.95	- 6.32	-6.24	-1.31	.81
8.96	7.48	-1.64	-4.12	9.17	7.39	-3.66	-3.42	5.37	3.52	-4.99	-2.53	- 7.58	-7.17	- .58	1.42
9.20	7.57	-2.46	-4.08	8.92	6.99	-4.35	-3.14	3.51	1.71	-5.08	-2.08	- 8.56	-7.91	.02	1.98
9.08	7.32	-3.34	-3.93	8.52	6.33	-4.86	-2.71	1.49	.09	-5.04	-1.56	- 9.33	-8.41	.69	2.50
8.64	6.78	-4.04	-3.70	7.81	5.32	-5.19	-2.25	- .50	-1.63	-4.83	- .91	- 9.91	-8.66	1.28	2.90
8.03	6.03	-4.64	-3.34	6.17	3.96	-5.38	-1.74	- 2.42	-3.27	-4.45	- .23	-10.20	-8.66	1.86	3.17
7.07	5.04	-5.04	-2.94	4.13	2.17	-5.37	-1.19	- 4.22	-4.83	-3.87	.48	-10.14	-8.21	2.41	3.32
5.61	3.67	-5.33	-2.48	2.19	.54	-5.17	- .60	- 5.80	-6.08	-3.11	1.18	- 9.73	-7.52	2.83	3.37
3.61	1.89	-5.41	-1.92	.18	-1.06	-4.74	0	- 7.16	-7.13	-2.41	1.87	- 8.92	-6.50	3.22	3.22
1.71	.28	-5.35	-1.35	- 1.68	-2.60	-4.17	.65	- 8.23	-7.88	-1.67	2.50	- 7.76	-5.41	3.46	2.93
- .15	-1.29	-5.12	- .74	- 3.57	-4.10	-3.41	1.35	- 9.04	-8.42	- .87	3.10	- 6.38	-4.19	3.59	2.48
- 1.93	-2.81	-4.67	- .07	- 5.11	-5.30	-2.58	2.06	- 9.62	-8.73	- .04	3.68	- 4.79	-2.77	3.68	1.90
- 3.69	-4.26	-4.05	.56	- 6.48	-6.28	-1.80	2.71	-10.00	-8.81	.78	3.99	- 3.01	-1.34	3.52	1.26
- 5.43	-5.66	-3.30	1.31	- 7.69	-7.12	- .93	3.28	-10.09	-8.60	1.63	4.20	- 1.27	.06	3.32	.56
- 6.83	-6.75	-2.43	2.04	- 8.62	-7.74	.04	3.74	- 9.83	-8.02	2.38	4.27	.57	1.54	2.86	- .13
- 7.98	-7.68	-1.64	2.78	- 9.38	-8.17	.91	4.05	- 9.12	-6.96	3.02	4.13	2.18	2.75	2.29	- .81
- 8.82	-8.17	- .78	3.39	- 9.92	-8.35	1.78	4.22	- 7.92	-5.70	3.56	3.87	3.68	3.86	1.68	-1.48
- 9.30	-8.48	.15	3.99	-10.12	-8.21	2.68	4.20	- 6.69	-4.38	4.02	3.42	5.04	4.90	.96	-2.02
- 9.97	-8.62	1.09	4.34	- 9.95	-7.67	3.30	4.02	- 4.84	-2.65	4.33	2.81	6.50	6.02	.18	-2.44
-10.10	-8.50	1.97	4.64	- 9.41	-6.99	3.92	3.66	- 2.61	- .81	4.44	2.05	7.61	6.83	- .55	-2.78
- 9.99	-8.04	2.81	4.75	- 8.51	-6.15	4.36	3.09	- .75	.67	4.35	1.15	8.52	7.50	-1.32	-2.98
- 9.44	-7.20	3.59	4.68	- 7.35	-5.04	4.71	2.40	1.14	2.23	4.07	.28	9.14	7.89	-1.99	-3.06
- 8.59	-6.24	4.26	4.48	- 5.73	-3.56	4.80	1.57	2.92	3.64	3.59	- .55	9.41	7.92	-2.71	-3.02
- 7.49	-5.13	4.79	4.05	- 3.75	-1.84	4.76	.68	4.53	4.78	2.93	-1.35	9.38	7.68		-2.92
- 6.04	-3.65	5.18	3.49	- 1.64	- .38	4.48	- .18	6.13	5.91	2.11	-2.10	8.97	7.09		-2.72
- 4.31	-2.06	5.34	2.73	.29	1.10	3.92	- .99	7.40	6.83	1.14	-2.76				
- 2.34	- .60	5.36	1.93	2.08	2.42		-1.81	8.46	7.56		-3.26				
- .53	.76	5.09	.95	3.57	3.83		-2.61	9.05	7.93		-3.57				
1.30	2.13	4.64	.22												
2.99	3.35	3.98	- .60												
4.69	4.42	3.18	-1.45												
6.10	5.38		-2.25												
7.22	6.28		-3.01												

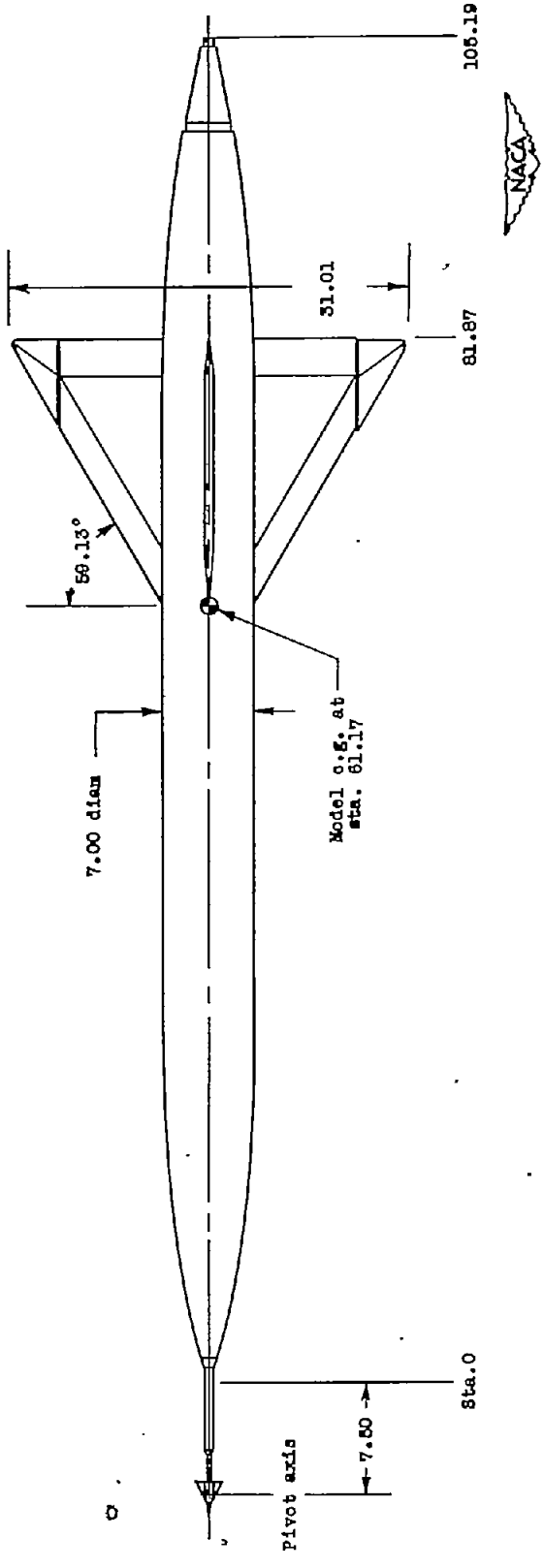

Figure 1.- Plan view of test vehicle. All dimensions in inches.

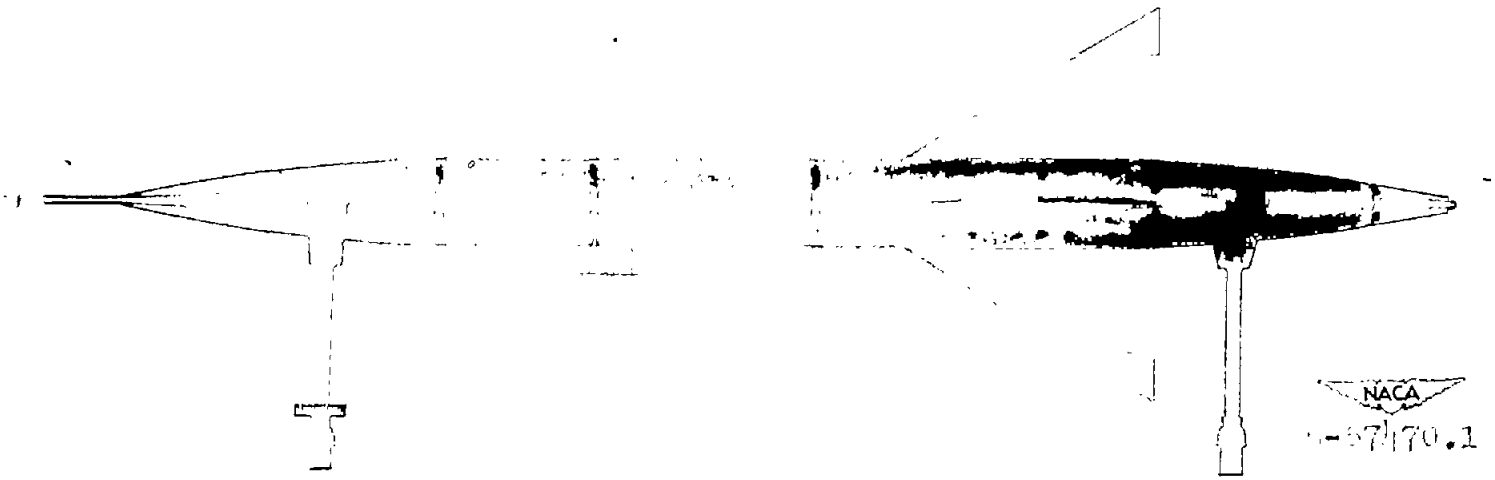

(a) Top view.

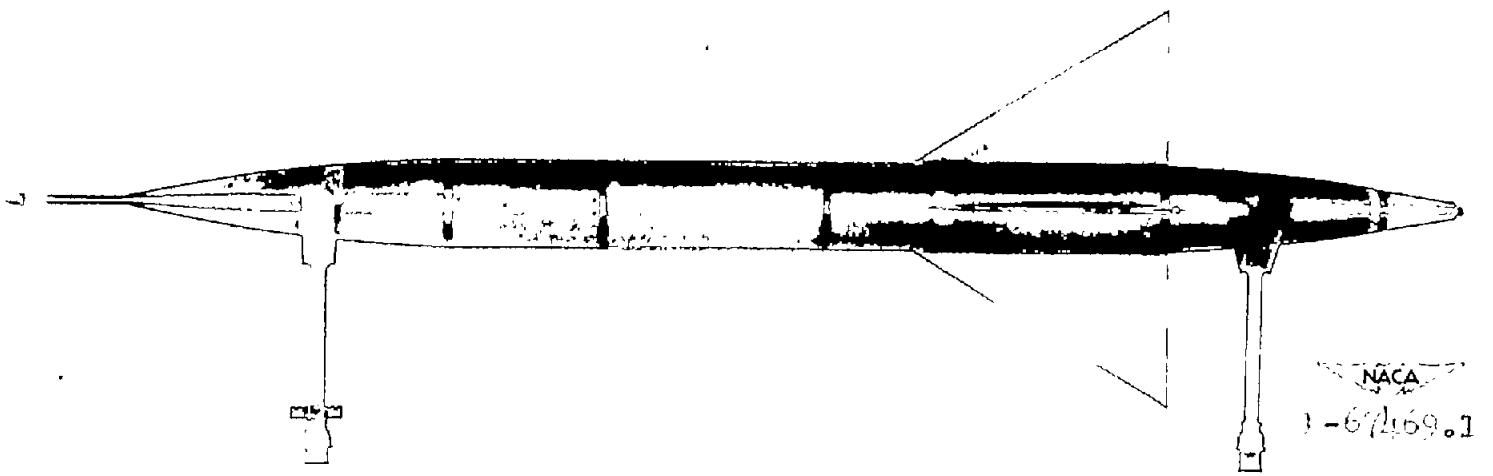

(b) Side view.

Figure 2.- Photographs of test vehicle.

(c) Preparatory to launching.

Figure 2.- Concluded.

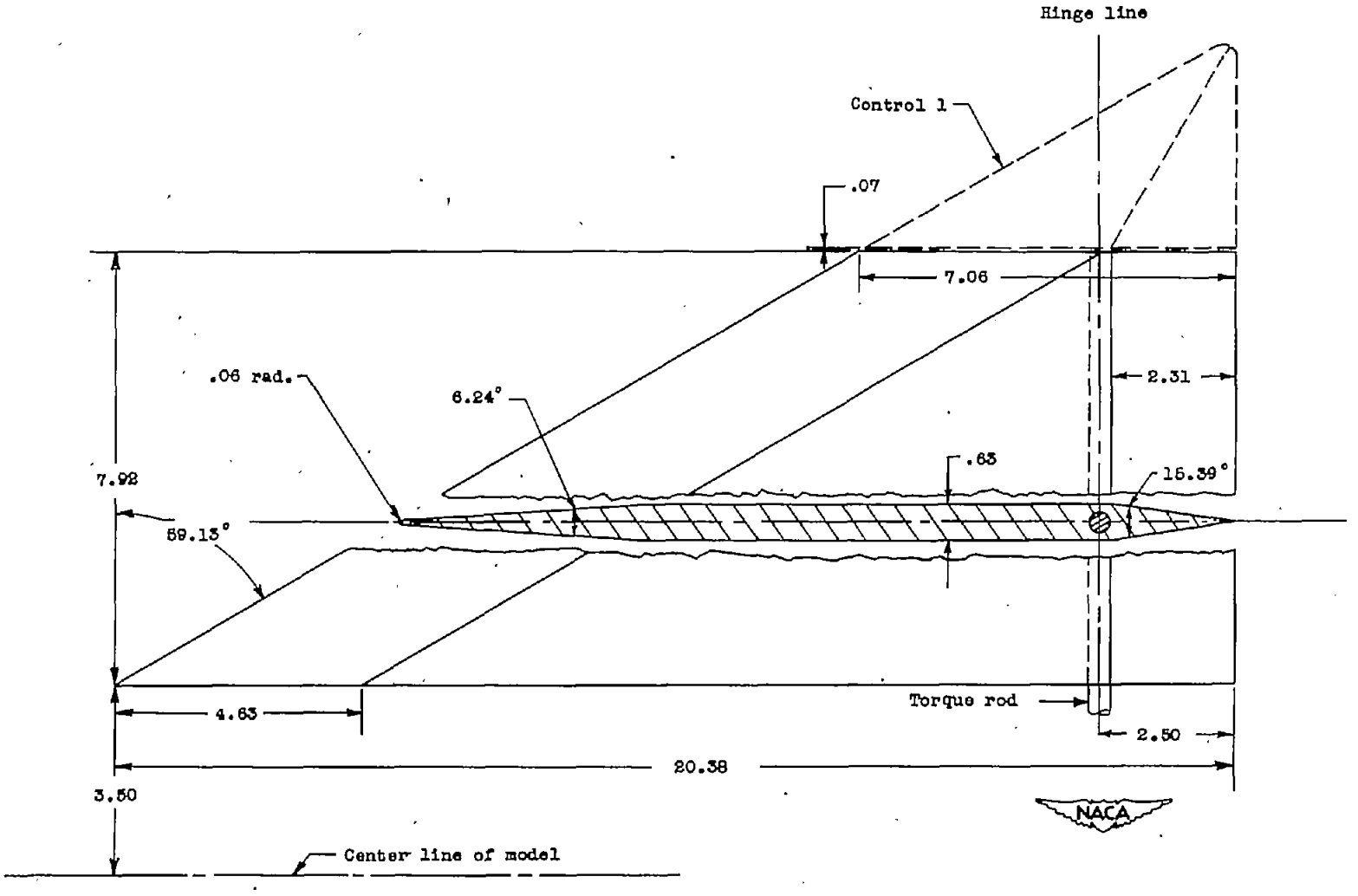

(a) Details of wing showing control 1 for reference.

Figure 3.- Control wing. (All dimensions in inches.)

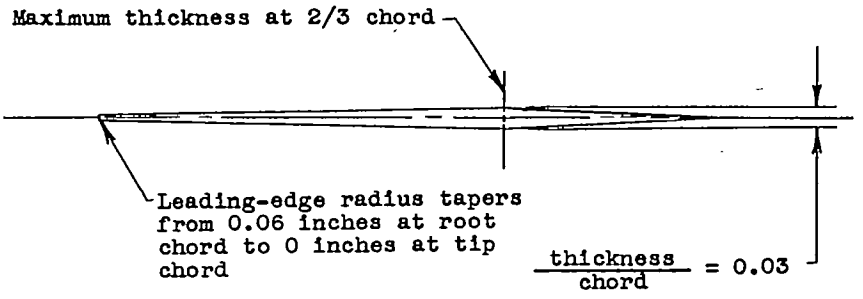

Section A-A

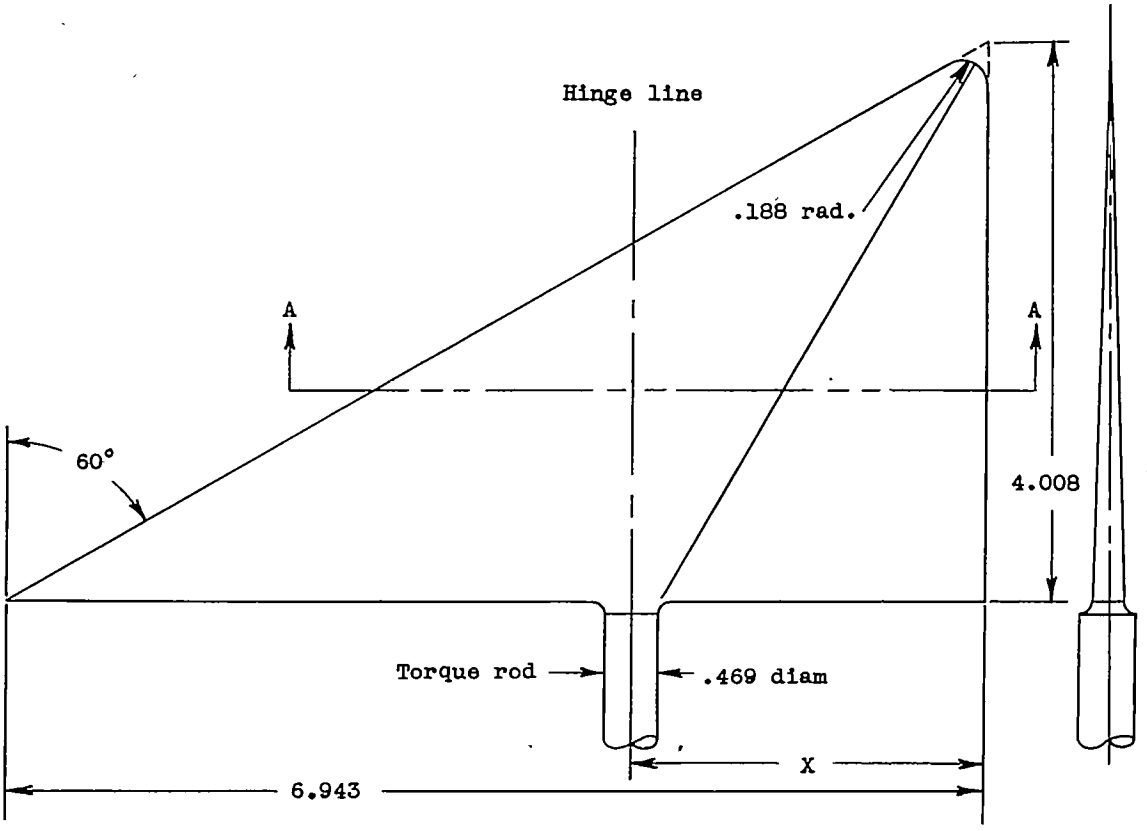

Control 1; X = 2.506 (hinge line at 0.6390 c_a)

Control 2; X = 2.163 (hinge line at 0.6885 c_a)

(b) Details of control.

Figure 3.- Concluded.

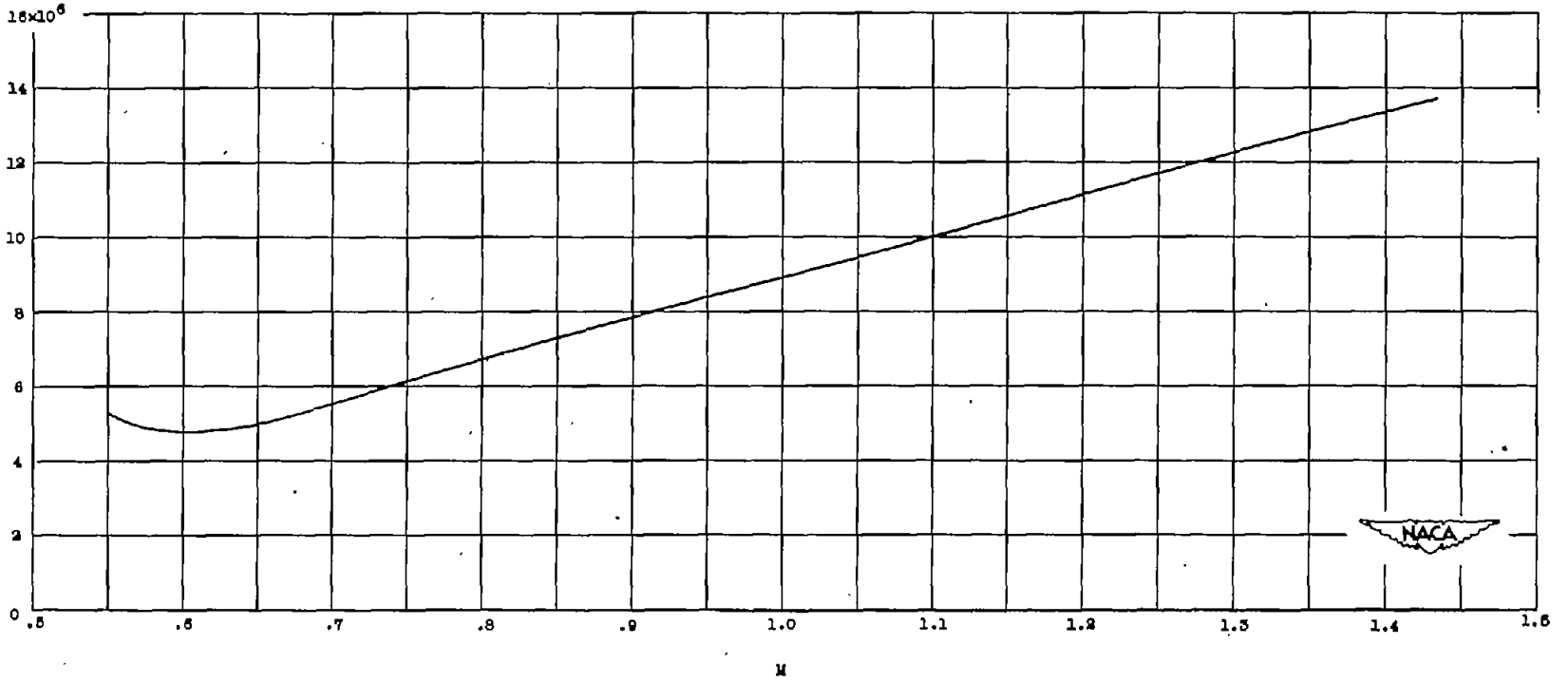

Figure 4.- Variation of Reynolds number with Mach number. Reynolds number is based on wing mean aerodynamic chord.

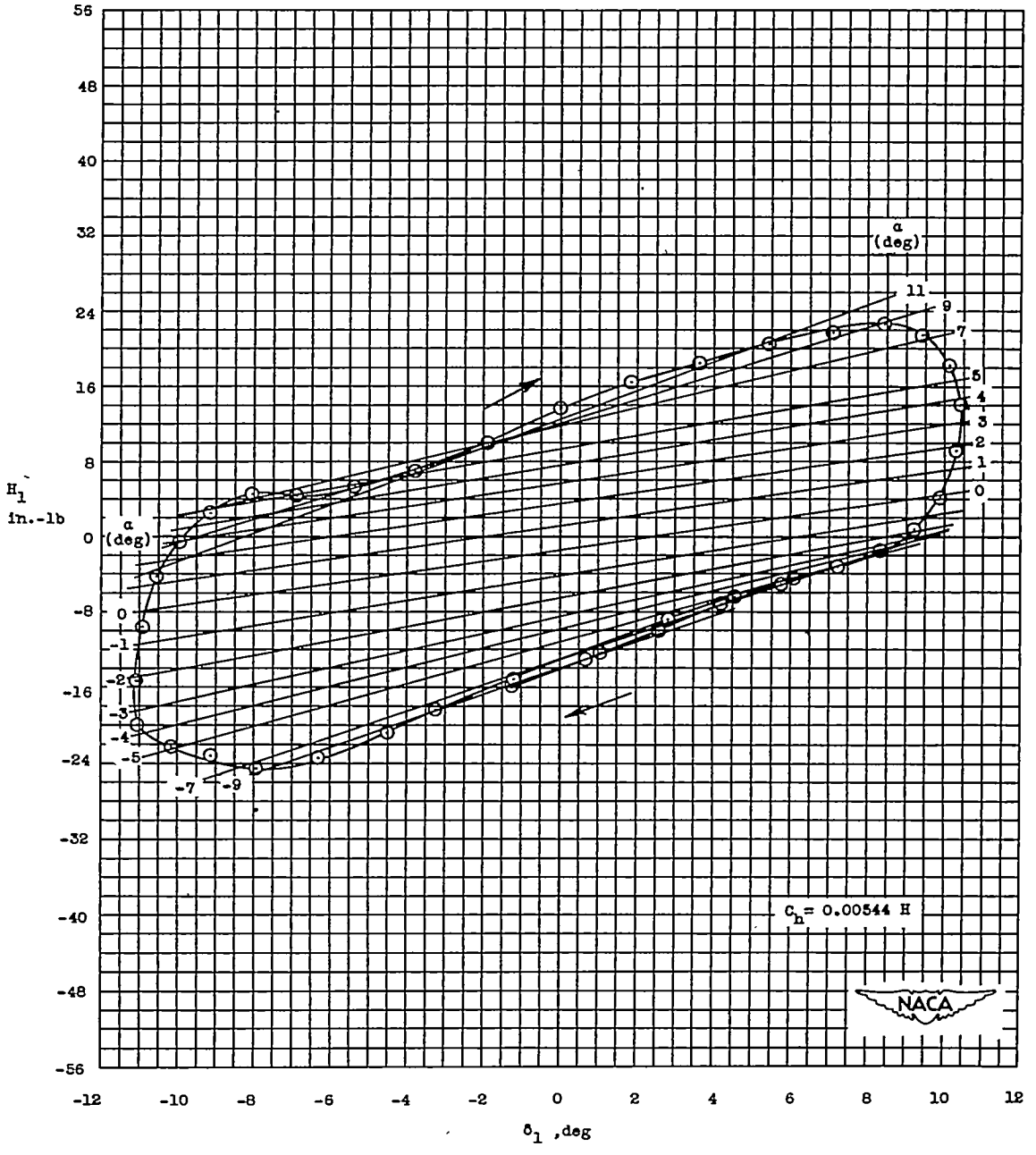

(a) M = 0.55; hinge line at 0.6390c_a.

Figure 5.- Variation of hinge-moment with control deflection, at various angles of attack, for two test hinge lines at several Mach numbers between 0.55 and 1.43. Arrows indicate time sequence of recorded data.

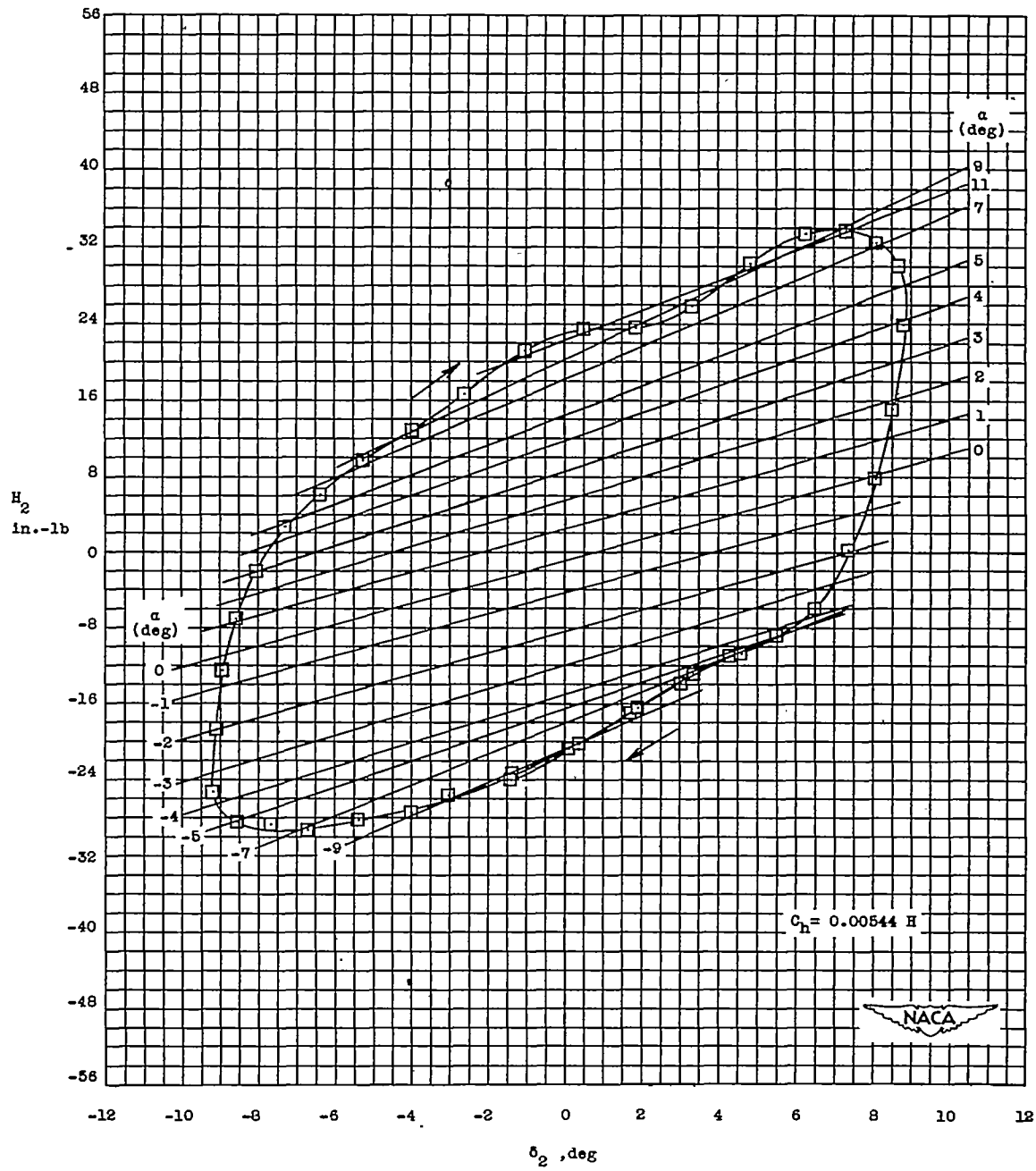

(b) M = 0.55; hinge line at 0.6885c_a.

Figure 5.- Continued.

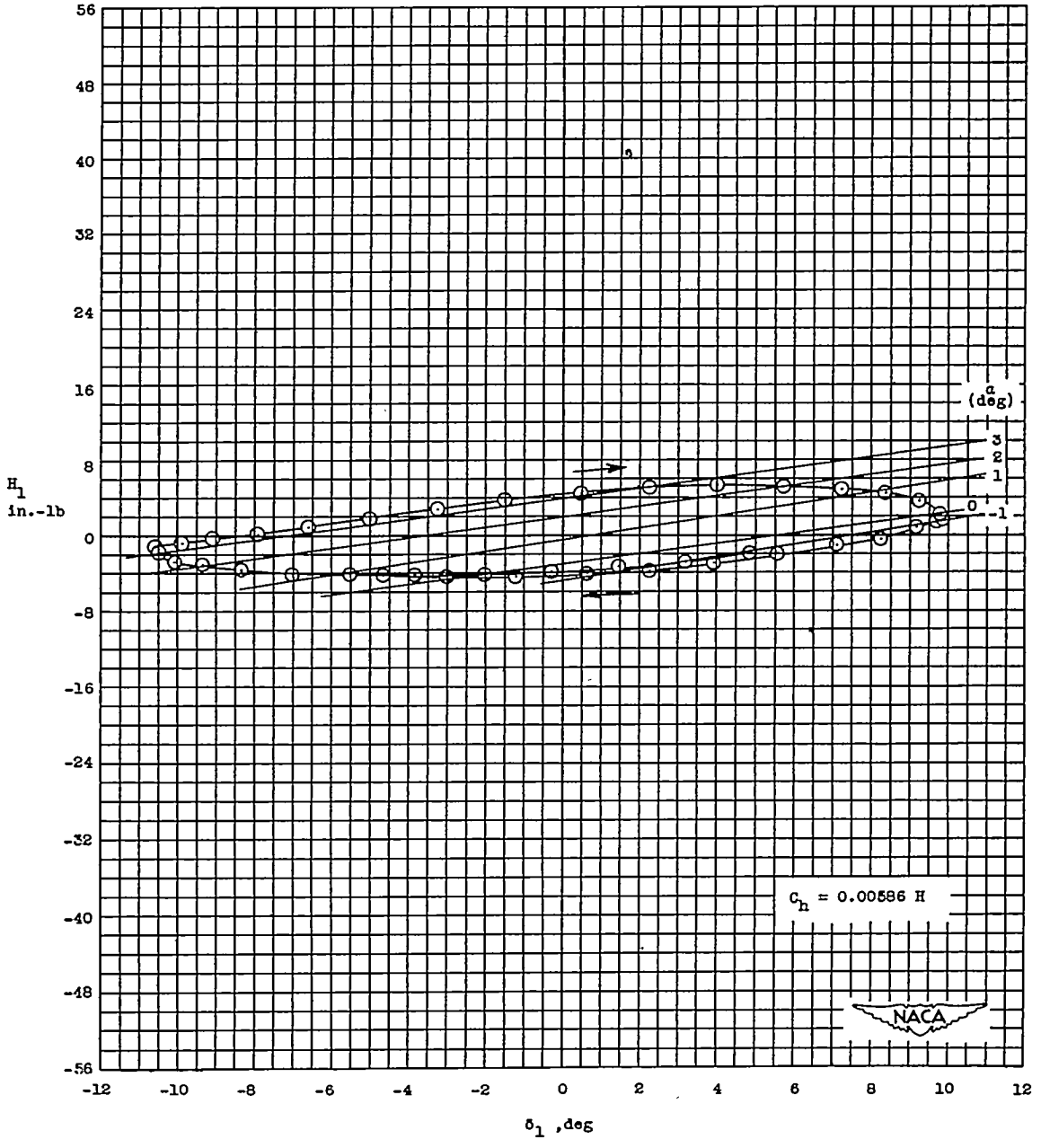

(c) M = 0.60; hinge line at $0.6390c_a$.

Figure 5.- Continued.

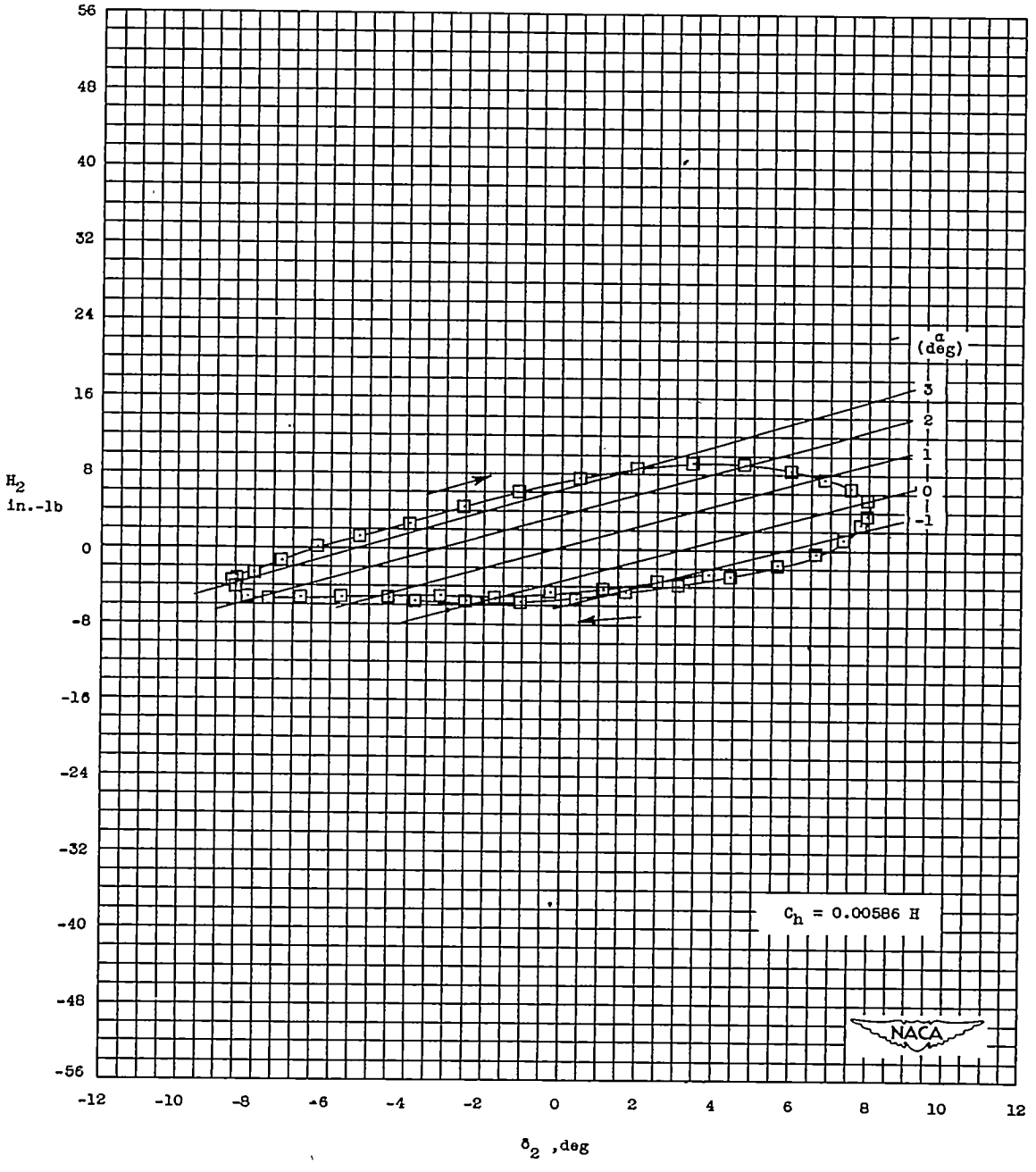

(d) M = 0.60; hinge line at $0.6885c_a$.

Figure 5.- Continued.

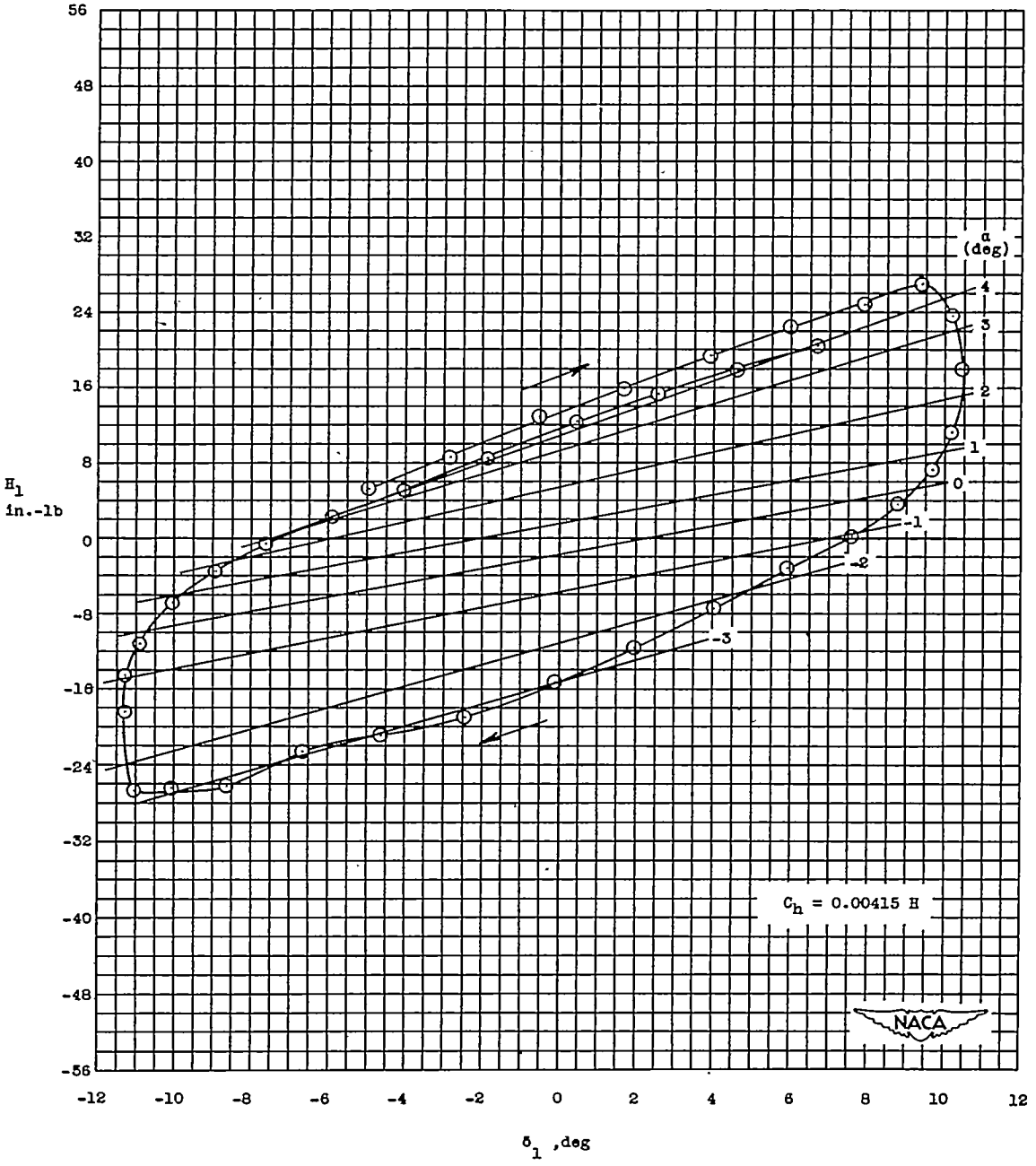

(e) M = 0.70; hinge line at $0.6390c_a$.

Figure 5.- Continued.

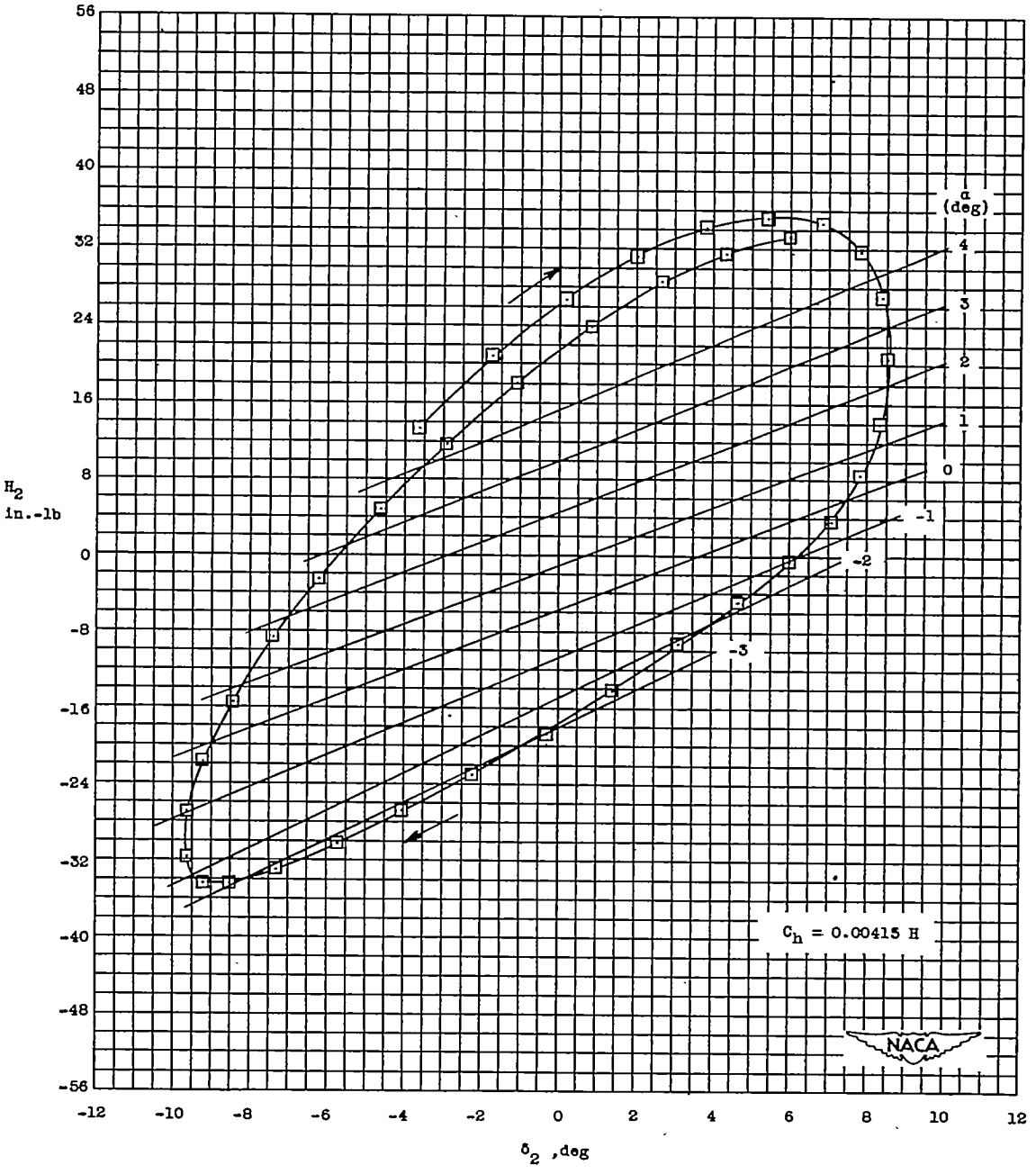

(f) M = 0.70; hinge line at $0.6885c_a$.

Figure 5.- Continued.

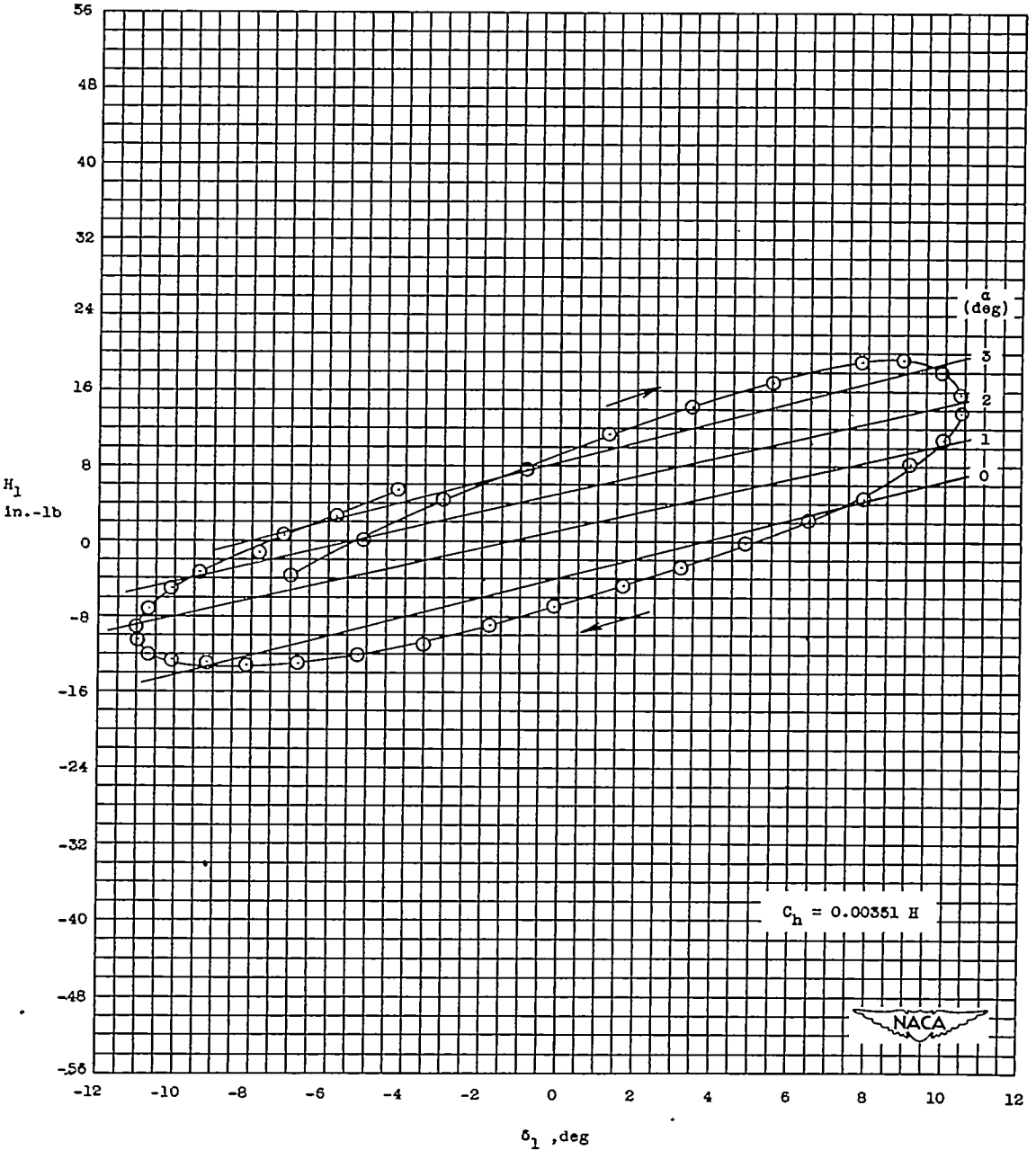

(g) M = 0.75; hinge line at 0.6390c_a.

Figure 5.- Continued.

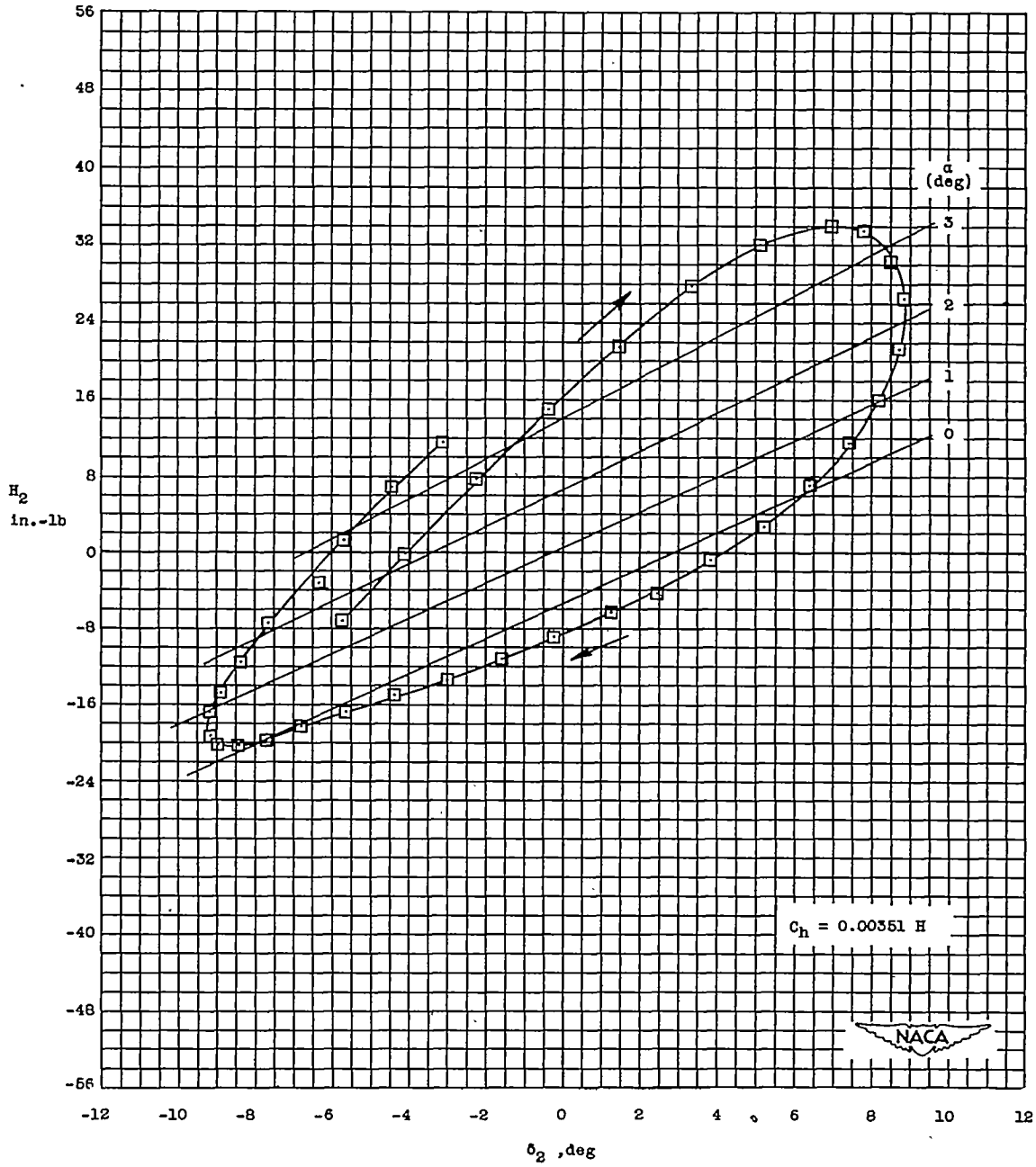

(h) M = 0.75; hinge line at $0.6885c_a$.

Figure 5.- Continued.

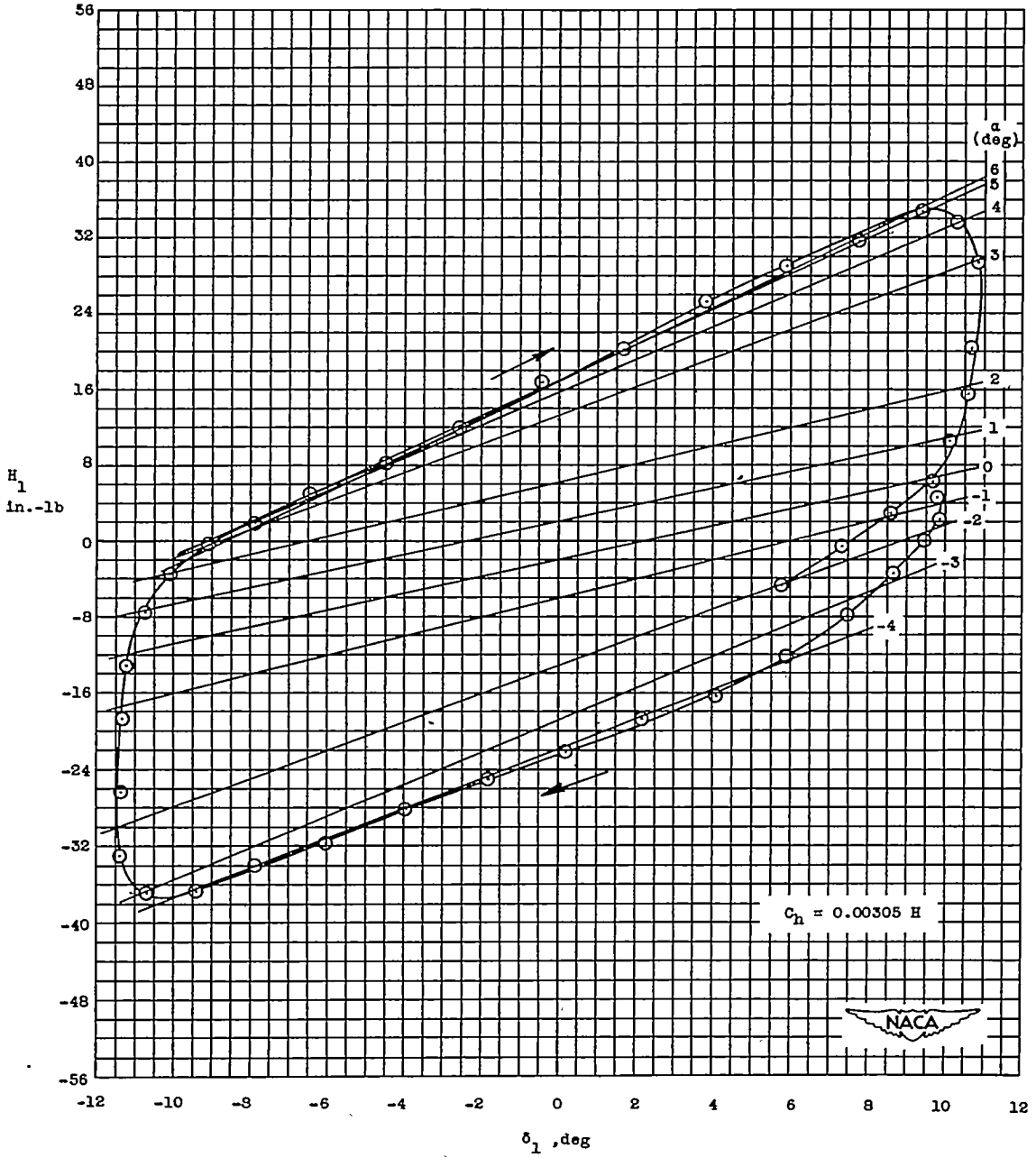

(i) M = 0.80; hinge line at $0.6390c_a$.

Figure 5.- Continued.

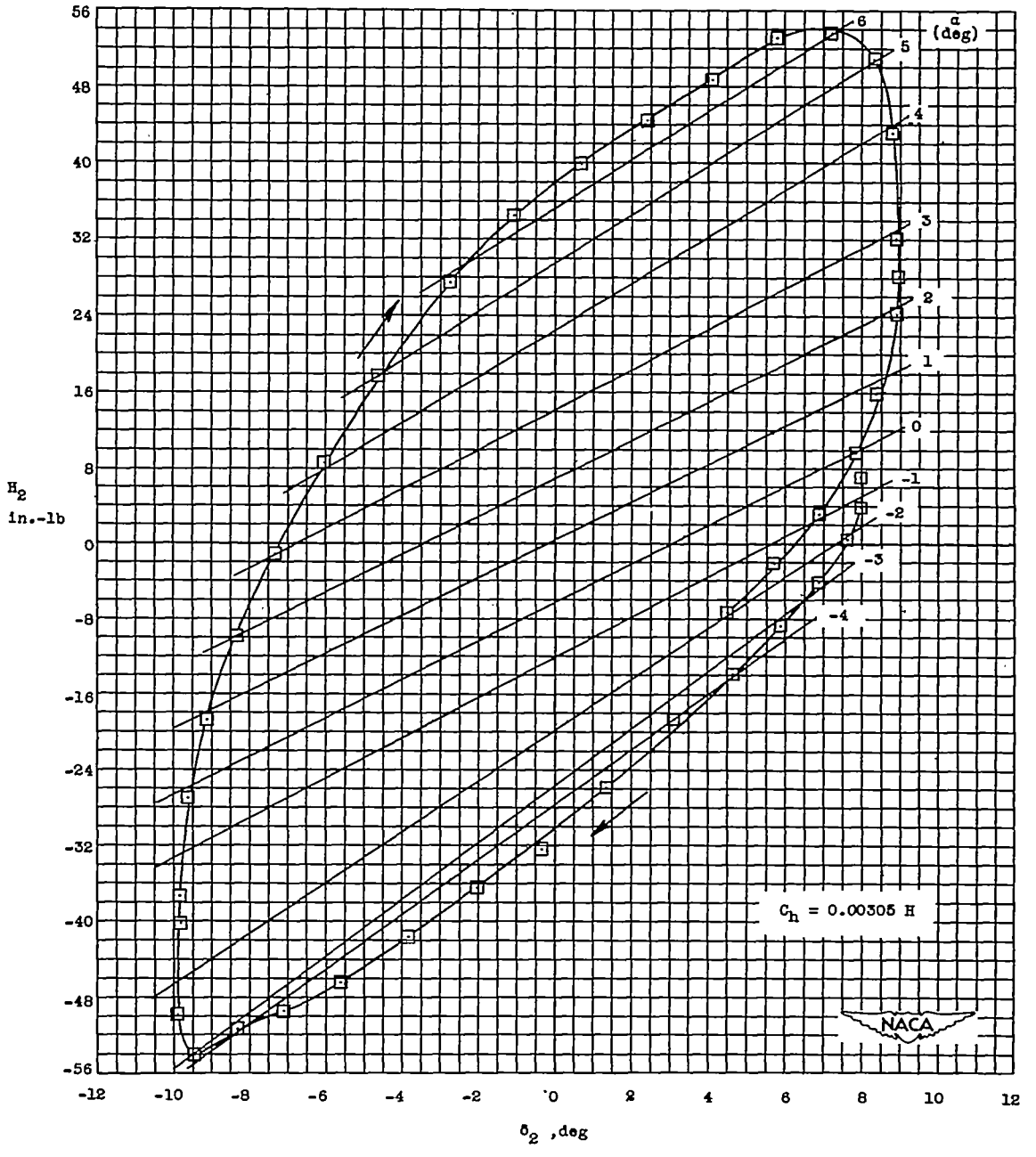

(j) M = 0.80; hinge line at $0.6885c_a$.

Figure 5.- Continued.

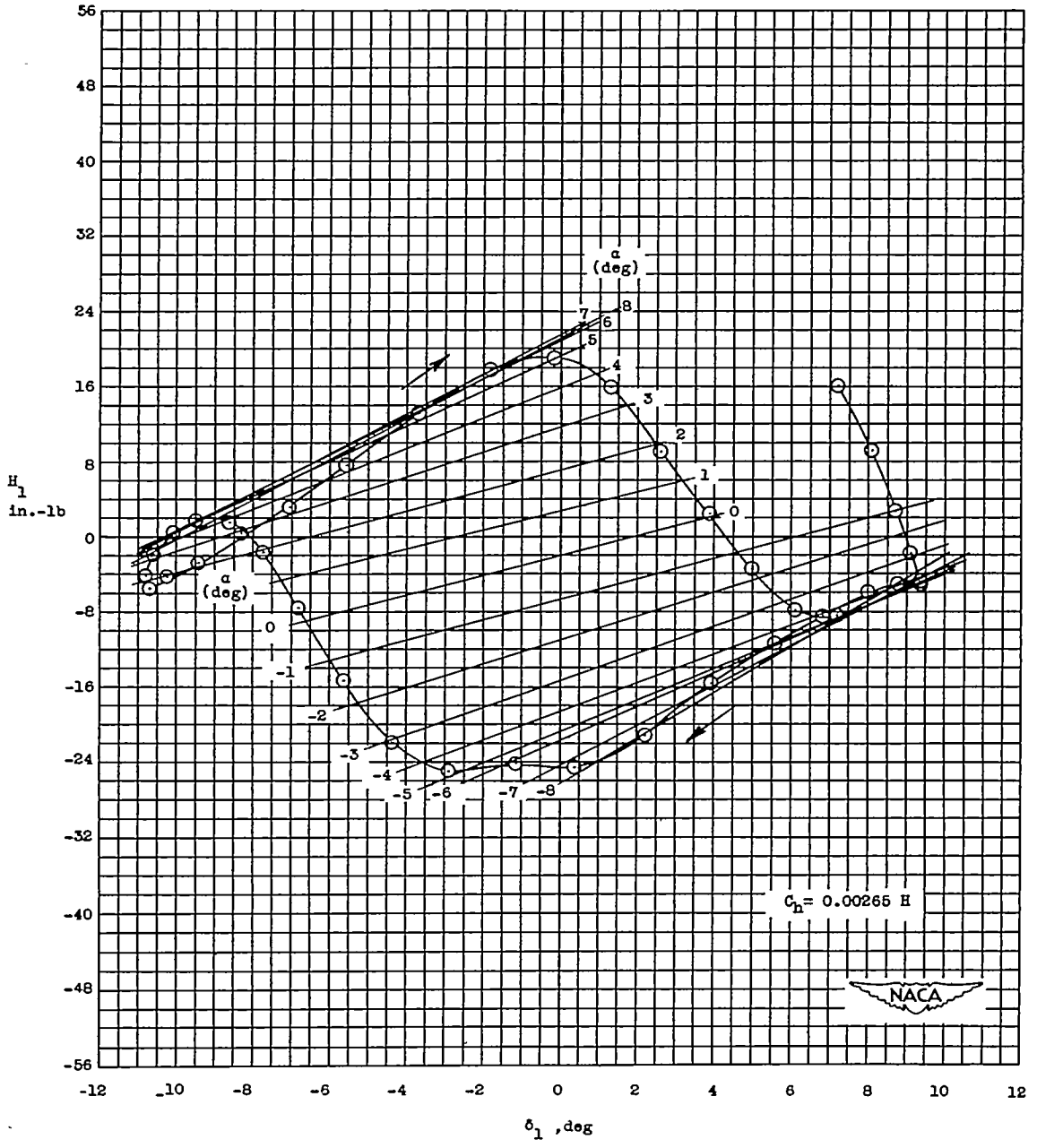

(k) M = 0.85; hinge line at 0.6390c_a.

Figure 5.- Continued.

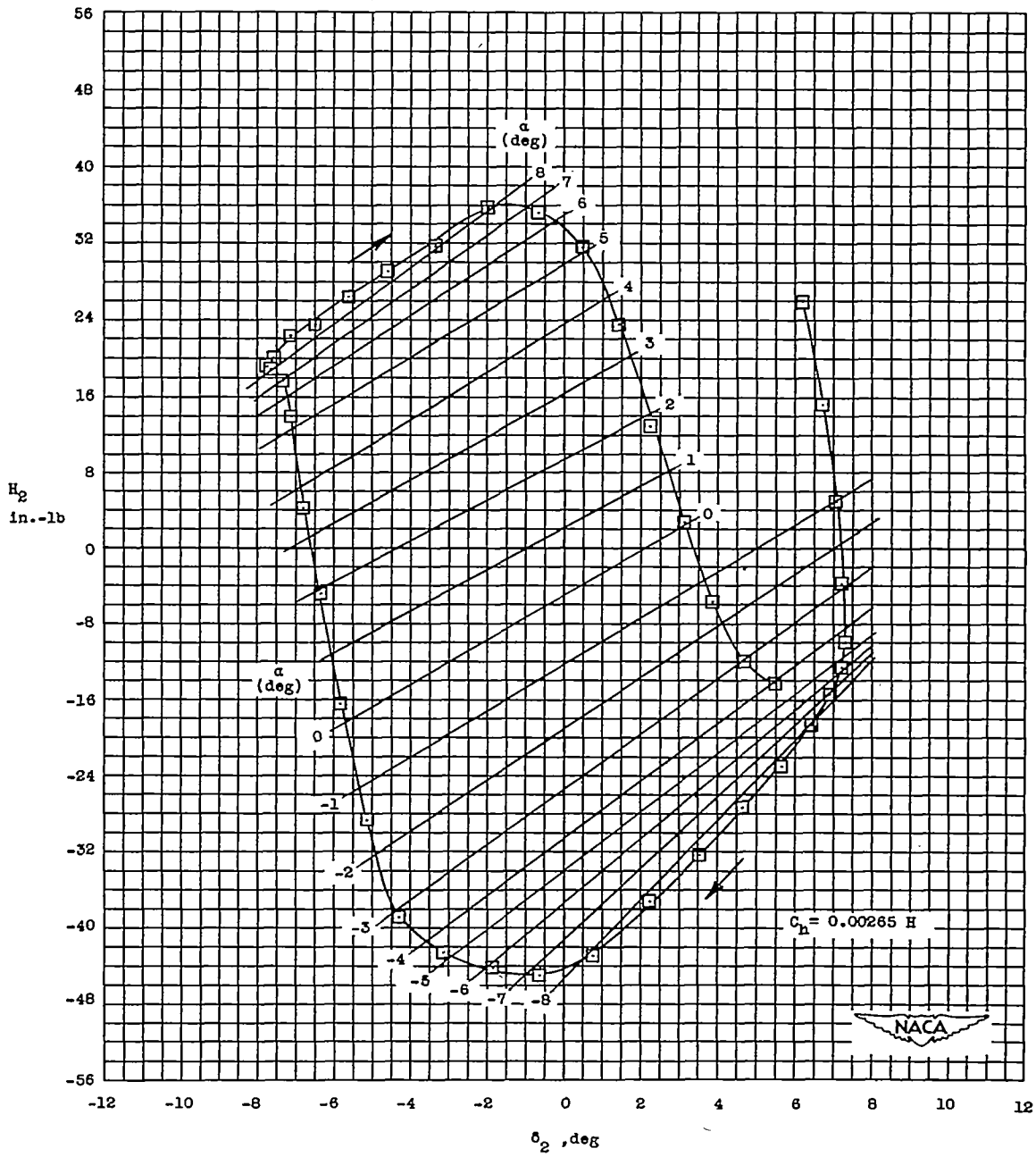

(l) M = 0.85; hinge line at $0.6885c_a$.

Figure 5.- Continued.

[redacted]

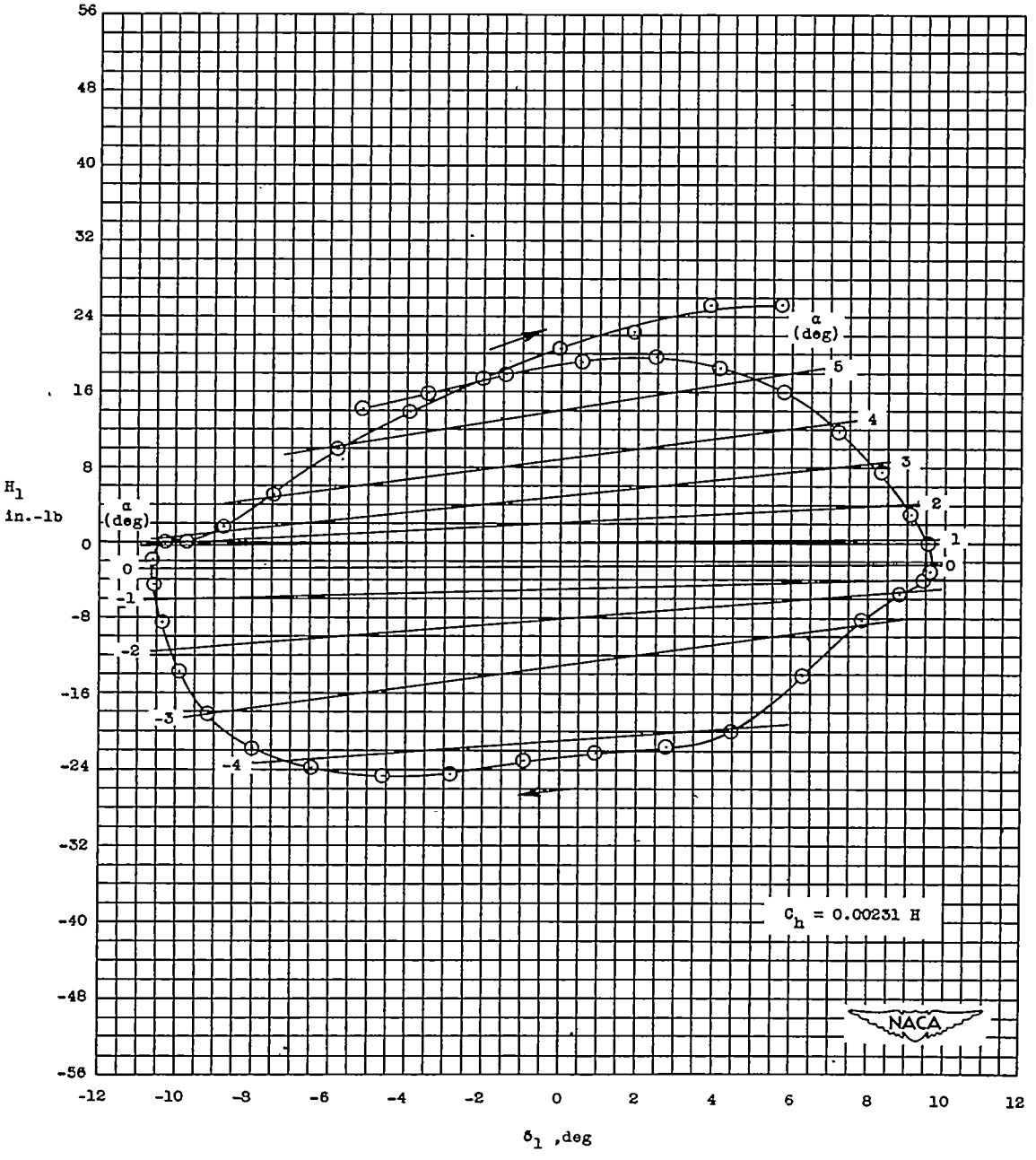

(m) M = 0.90; hinge line at $0.6390c_a$.

Figure 5.- Continued.

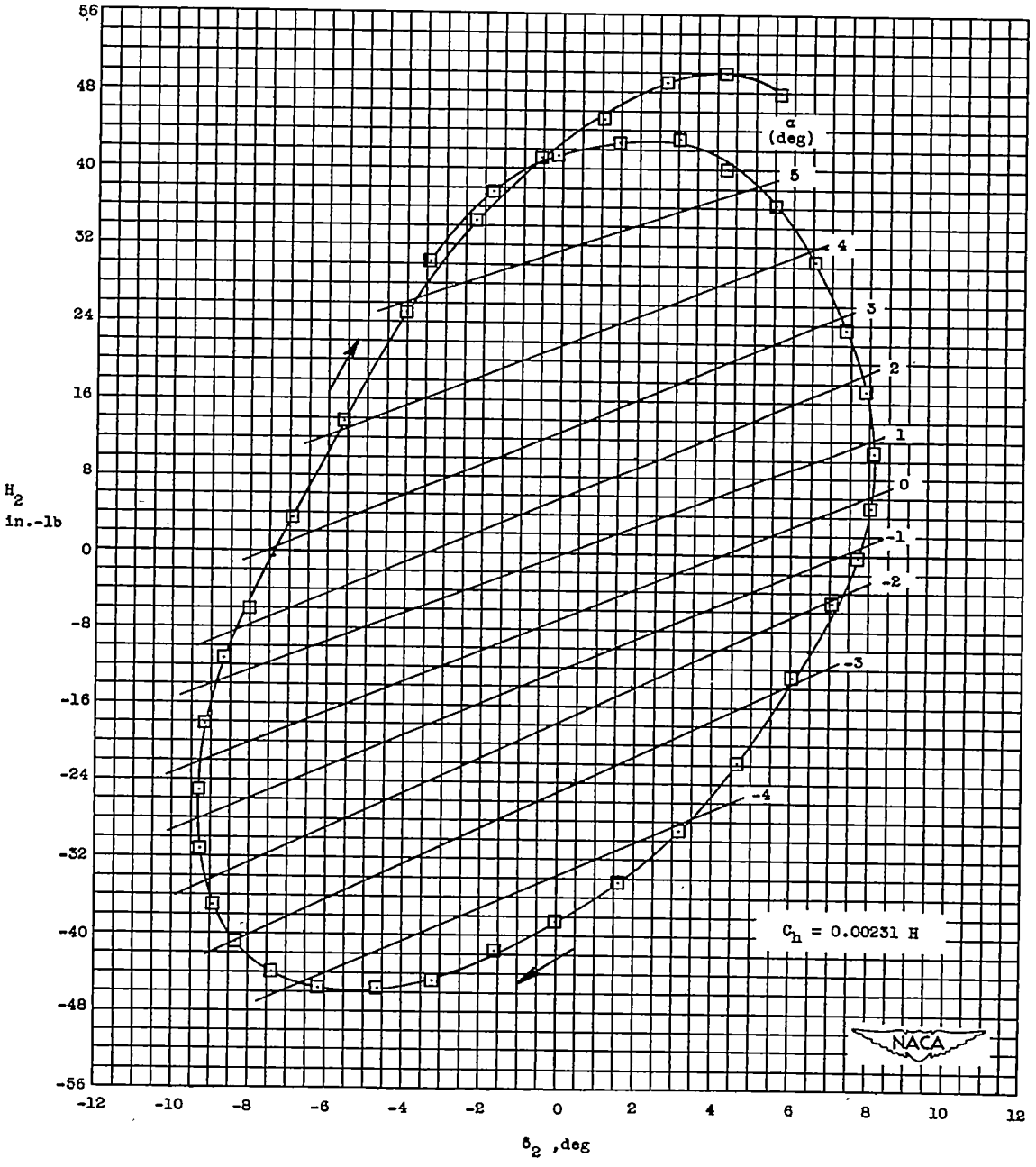

(n) M = 0.90; hinge line at $0.6885c_a$.

Figure 5.- Continued.

[redacted]

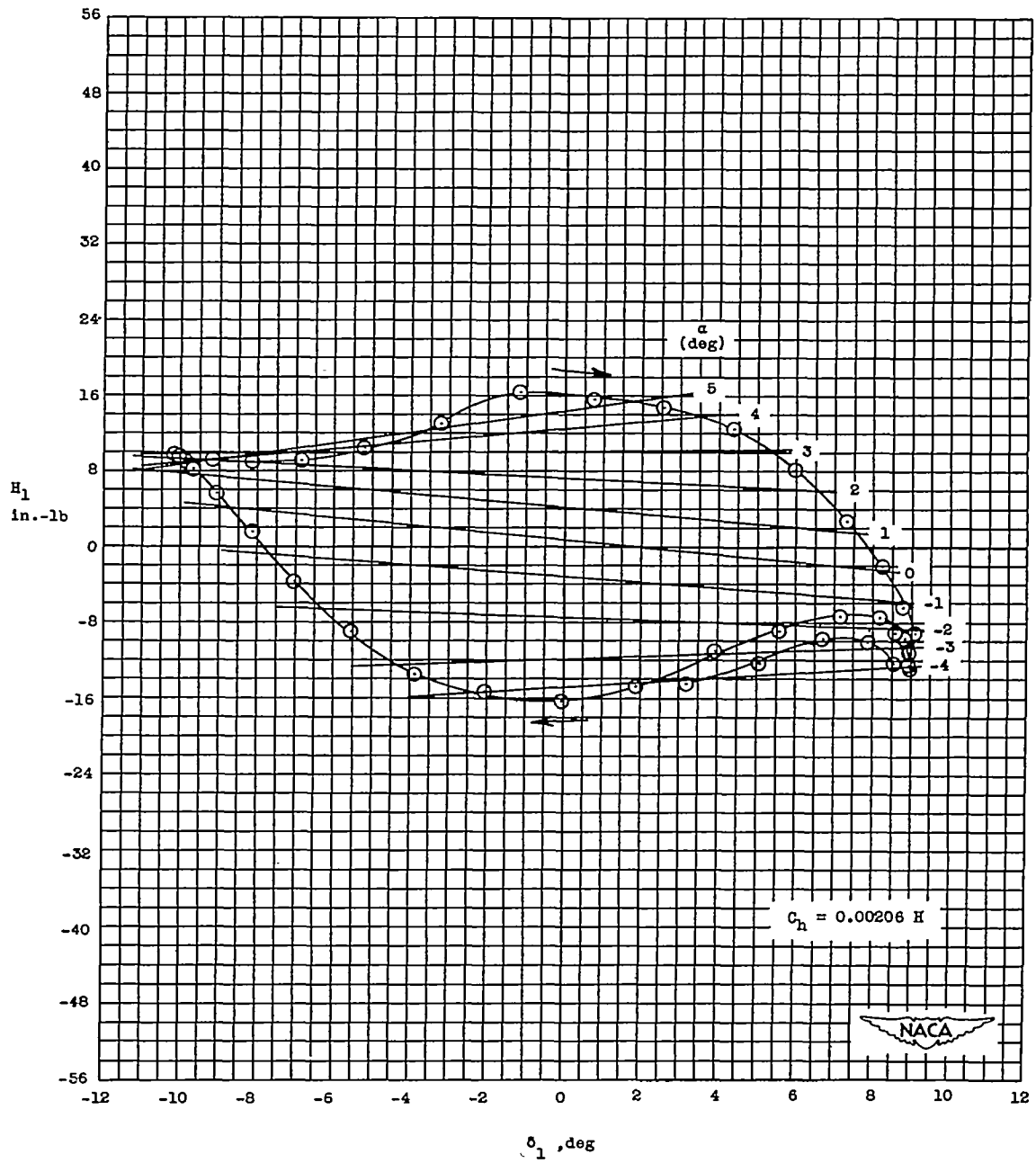

(o) M = 0.95; hinge line at $0.6390c_a$.

Figure 5.- Continued.

[redacted]

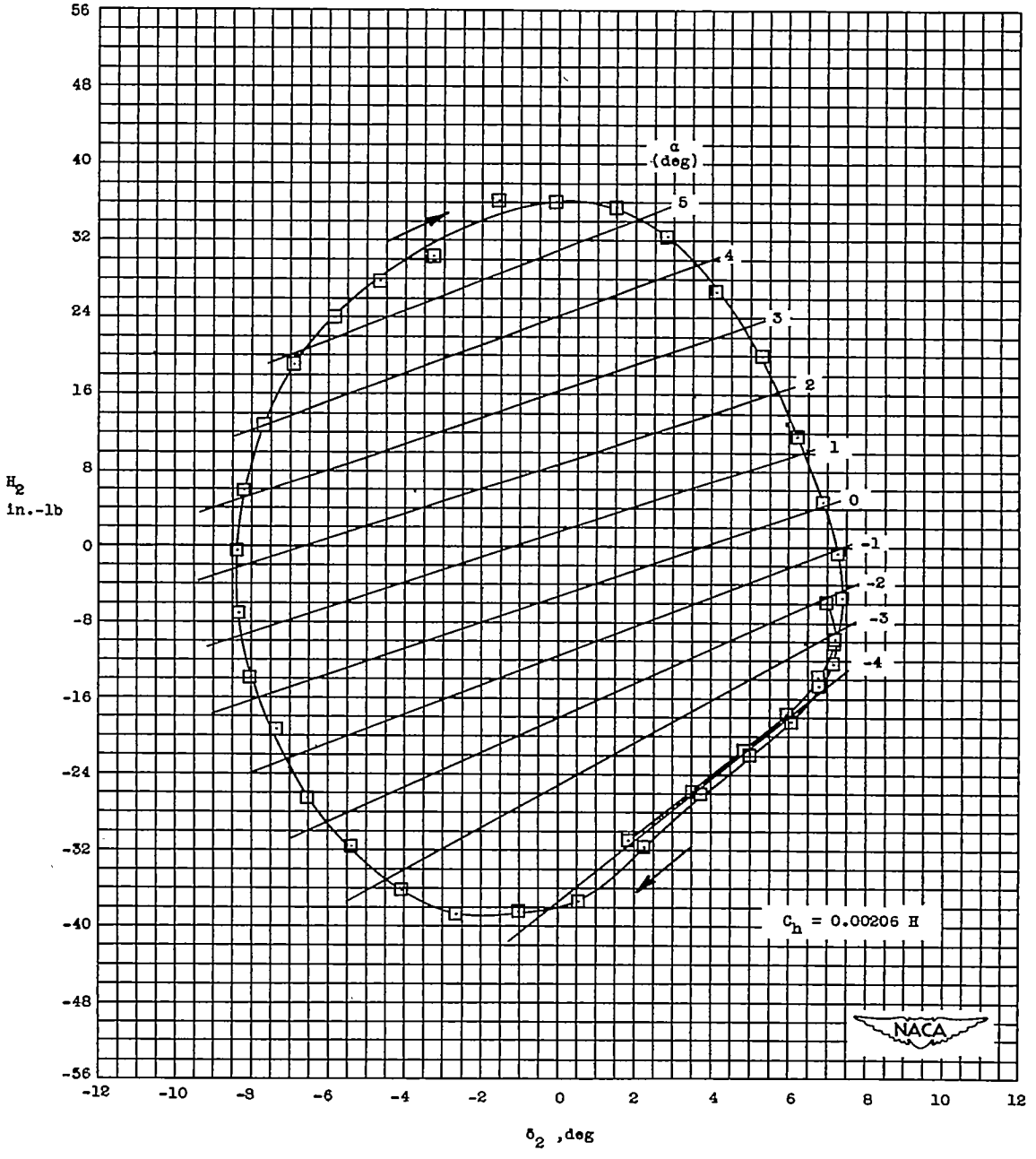

(p) M = 0.95; hinge line at 0.6885c_a.

Figure 5.- Continued.

[redacted]

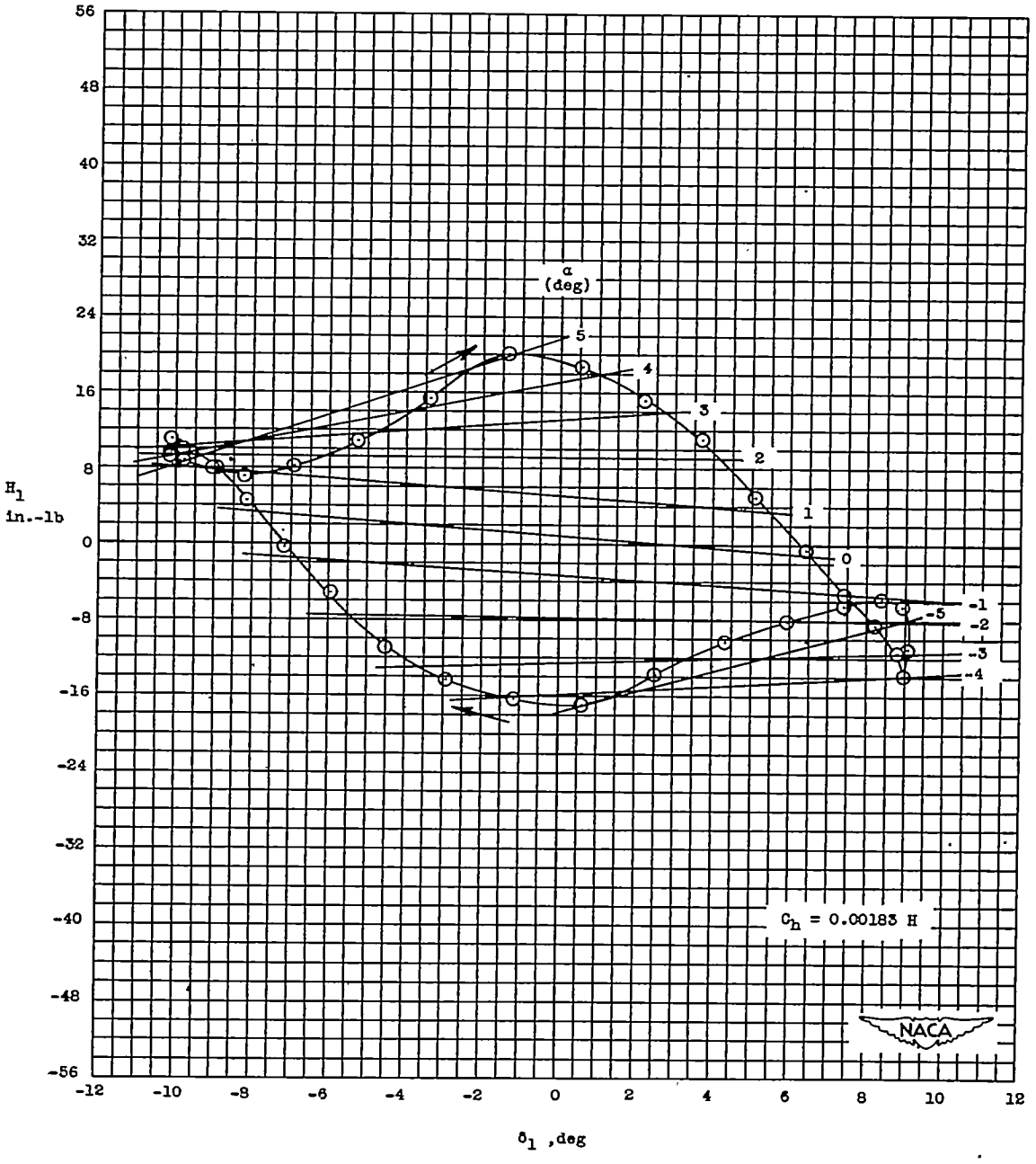

(q) M = 1.00; hinge line at $0.6390c_a$.

Figure 5.- Continued.

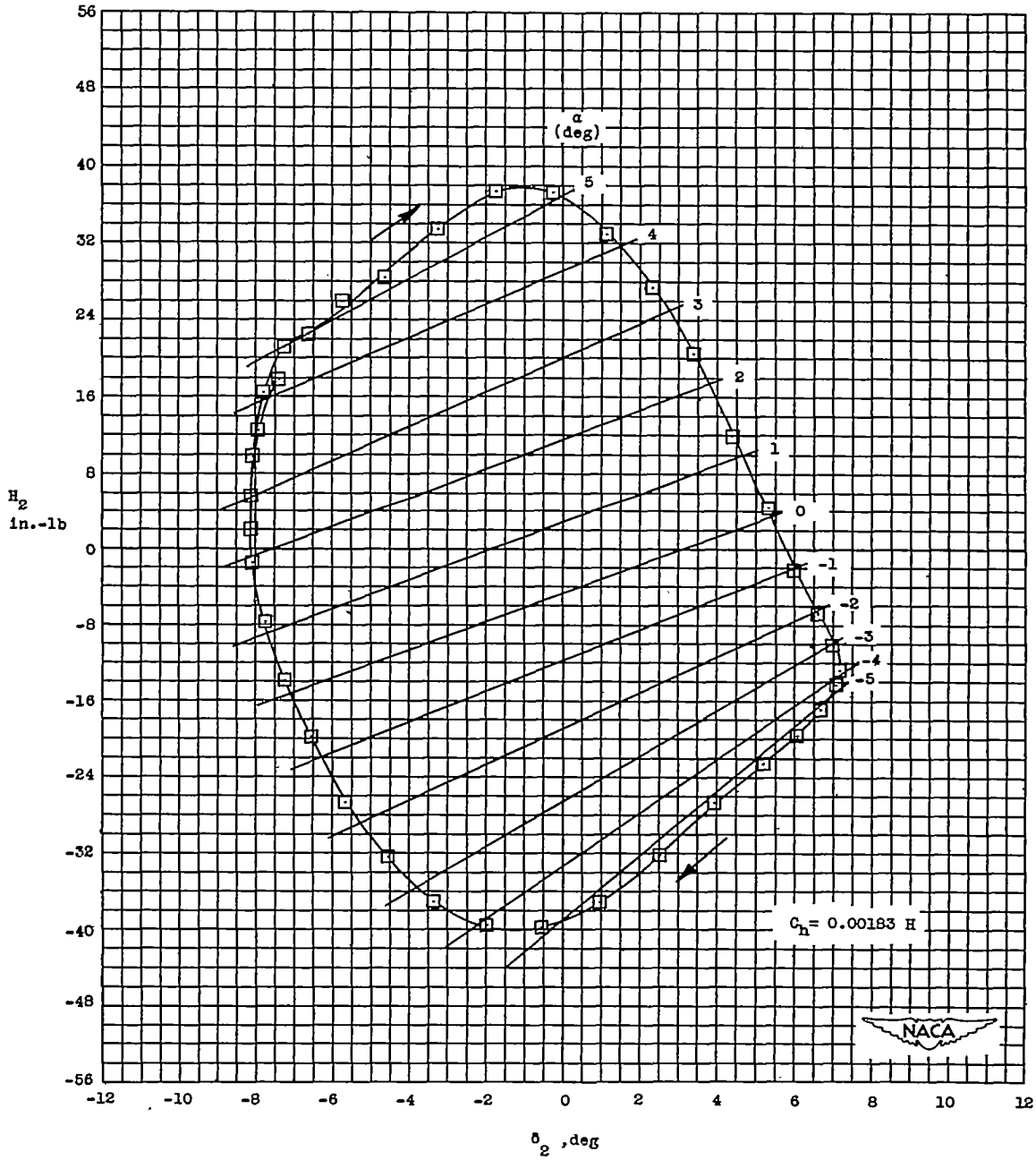

(r) M = 1.00; hinge line at 0.6885c_a.

Figure 5.- Continued.

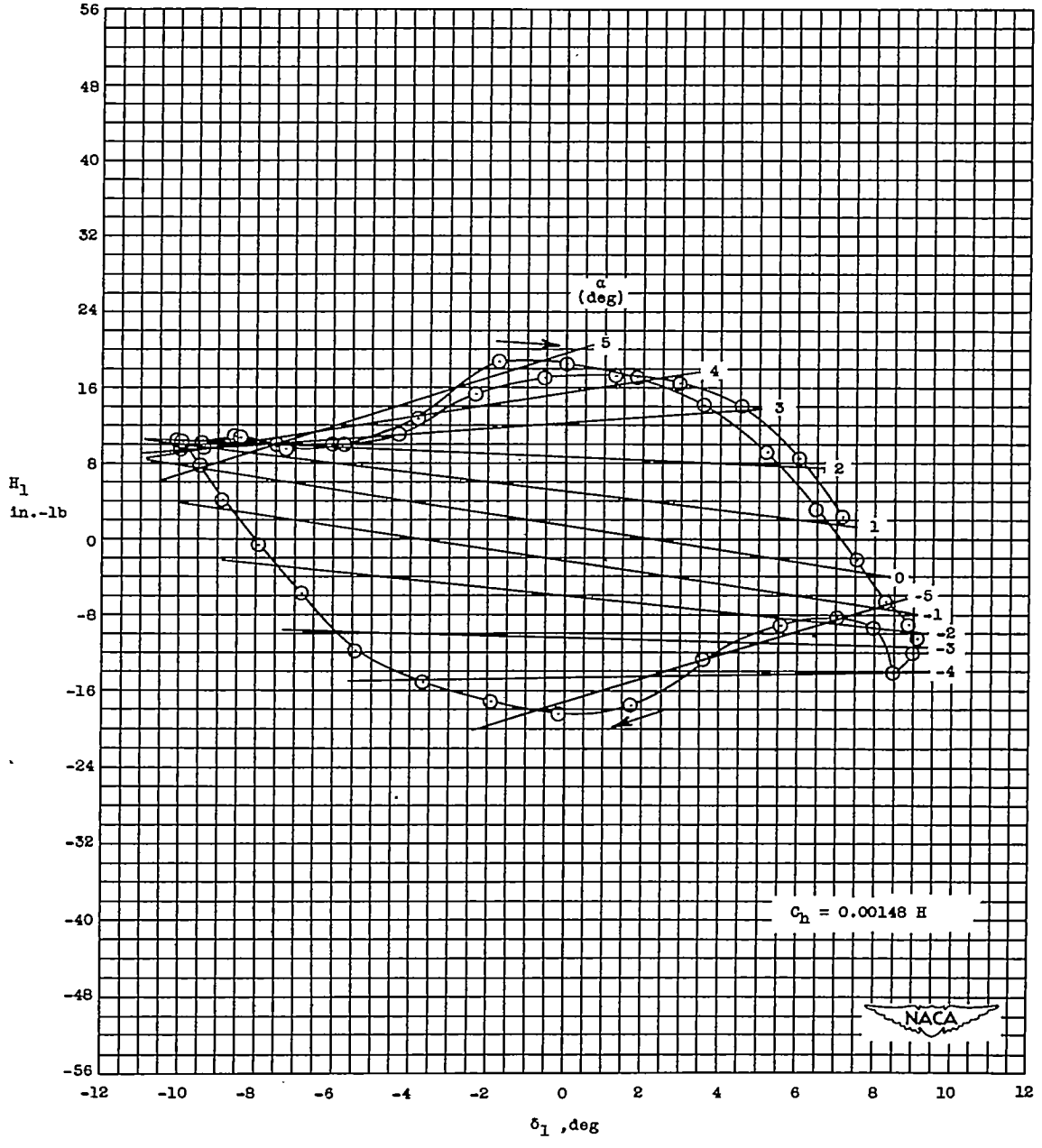

(s) M = 1.10; hinge line at 0.6390c_a.

Figure 5.- Continued.

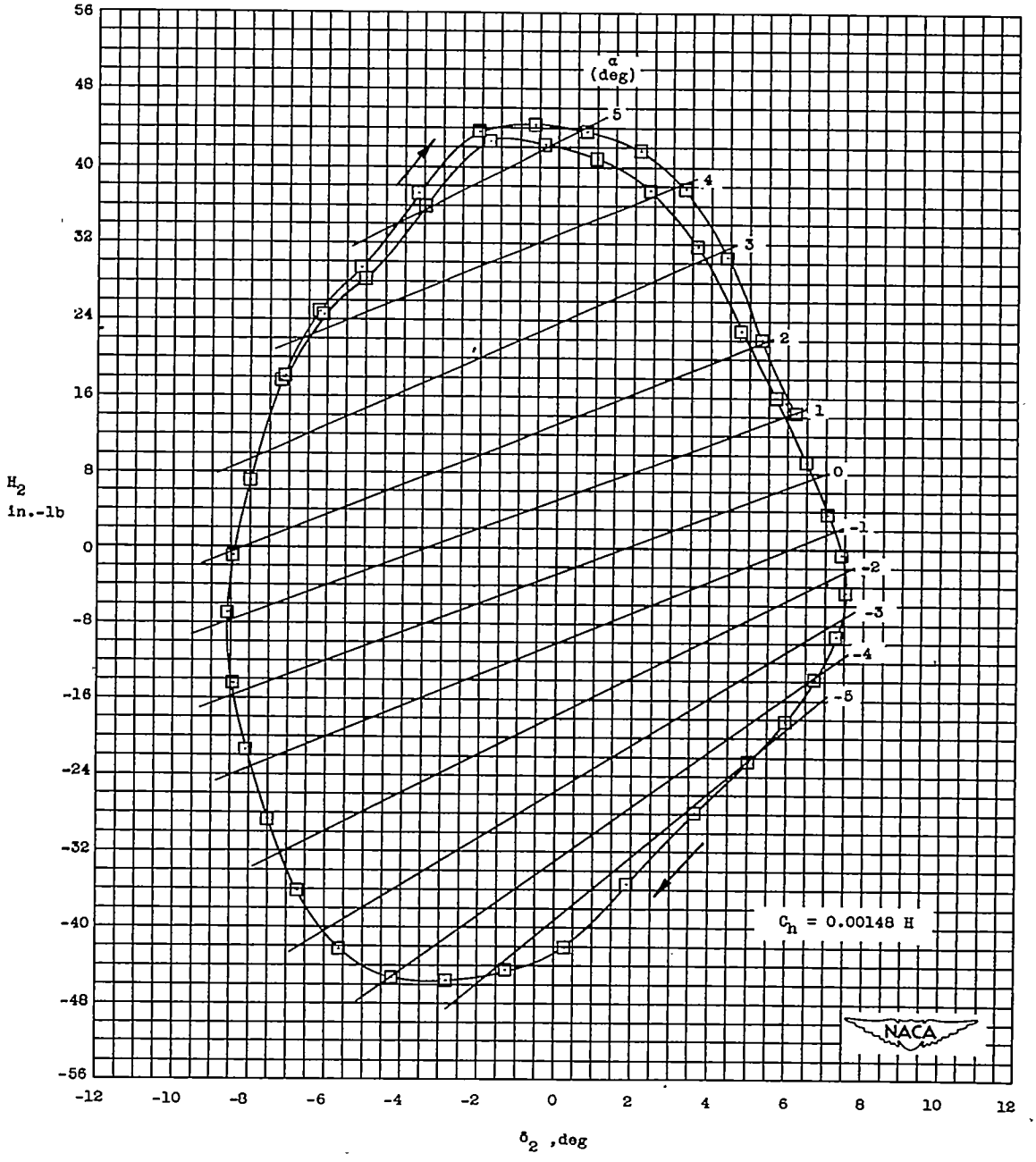

(t) M' = 1.10; hinge line at $0.6885c_a$.

Figure 5.- Continued.

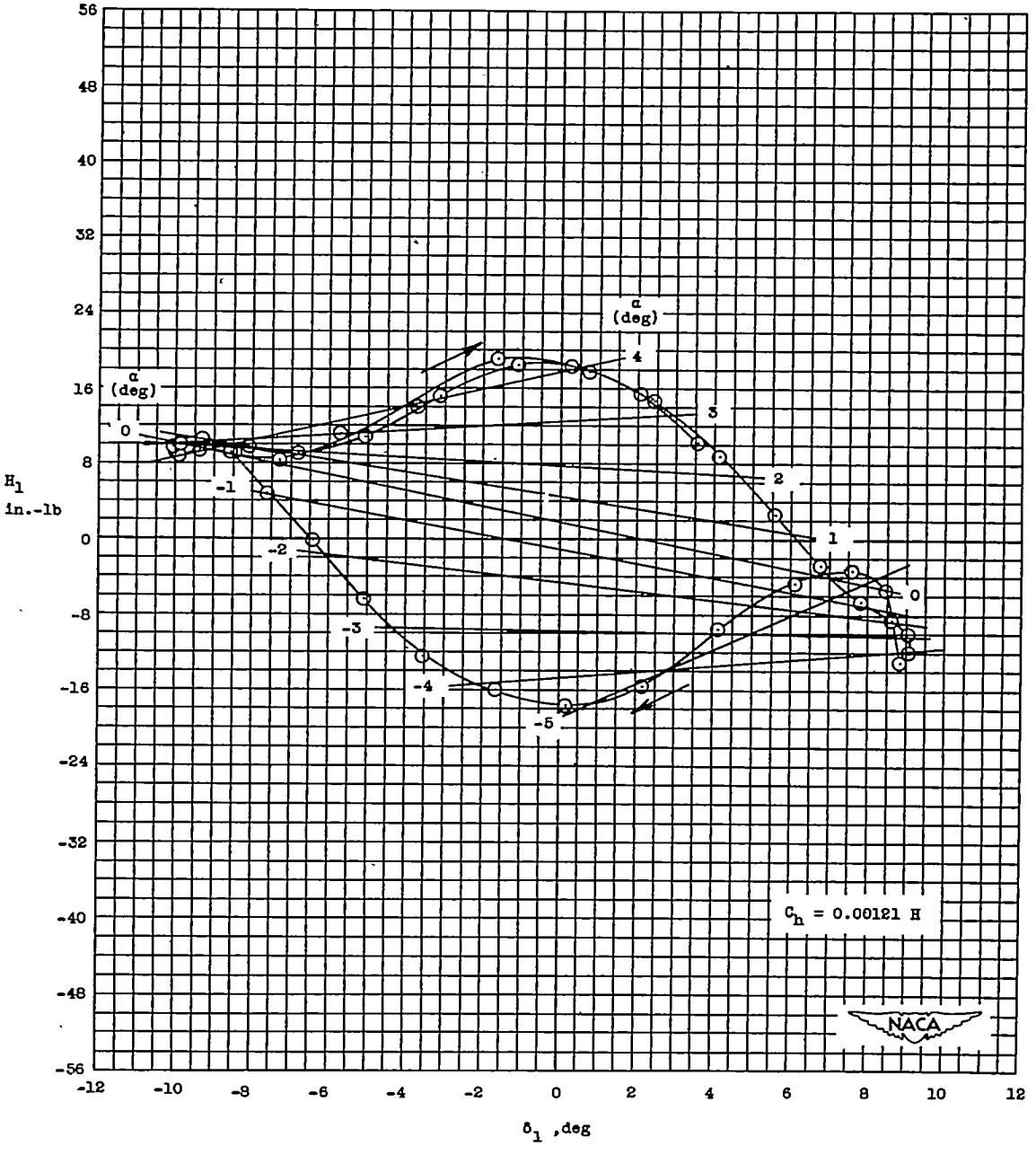

(u) M = 1.20; hinge line at $0.6390c_a$.

Figure 5.- Continued.

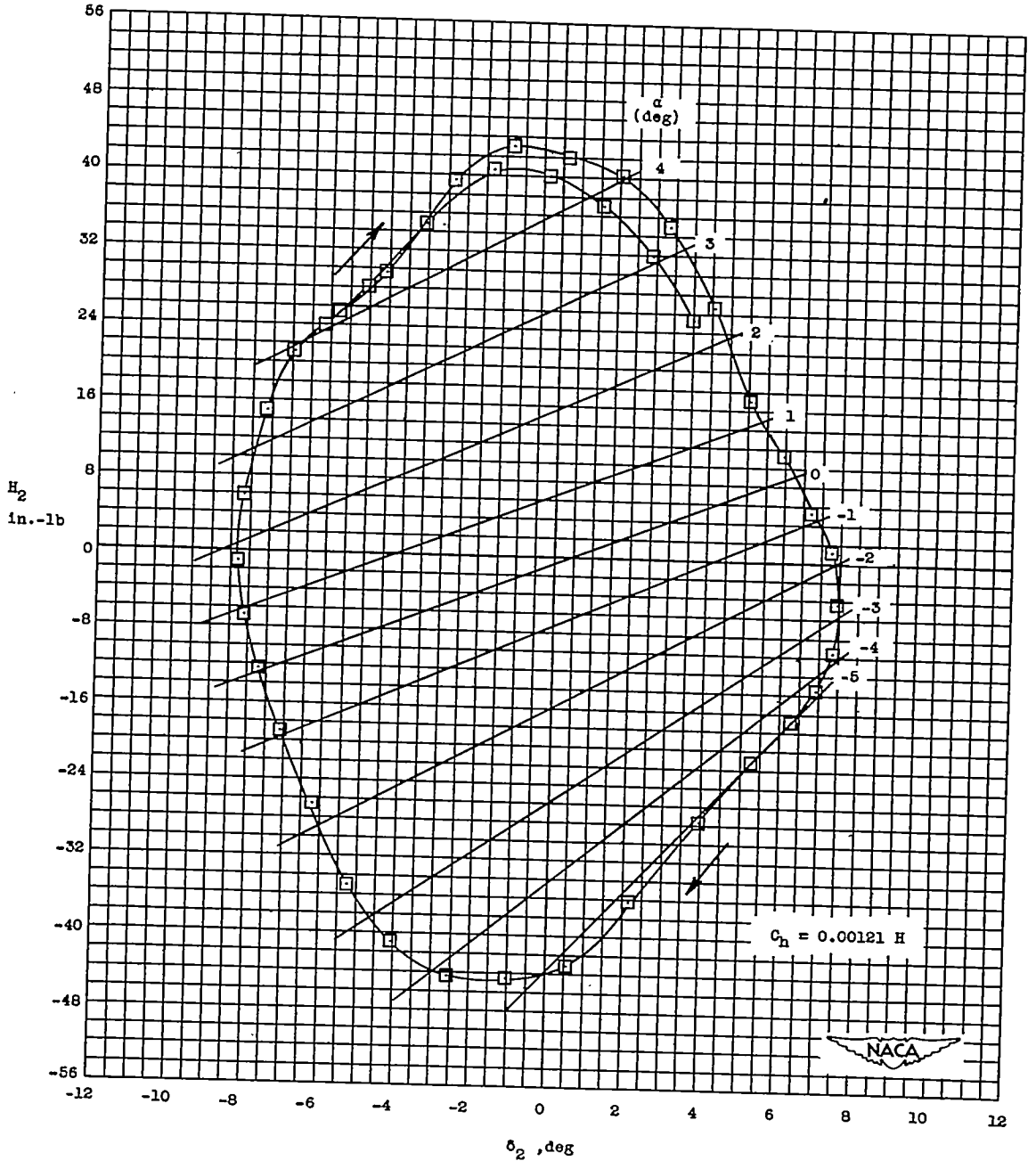

(v) M = 1.20; hinge line at $0.6885c_a$.

Figure 5.- Continued.

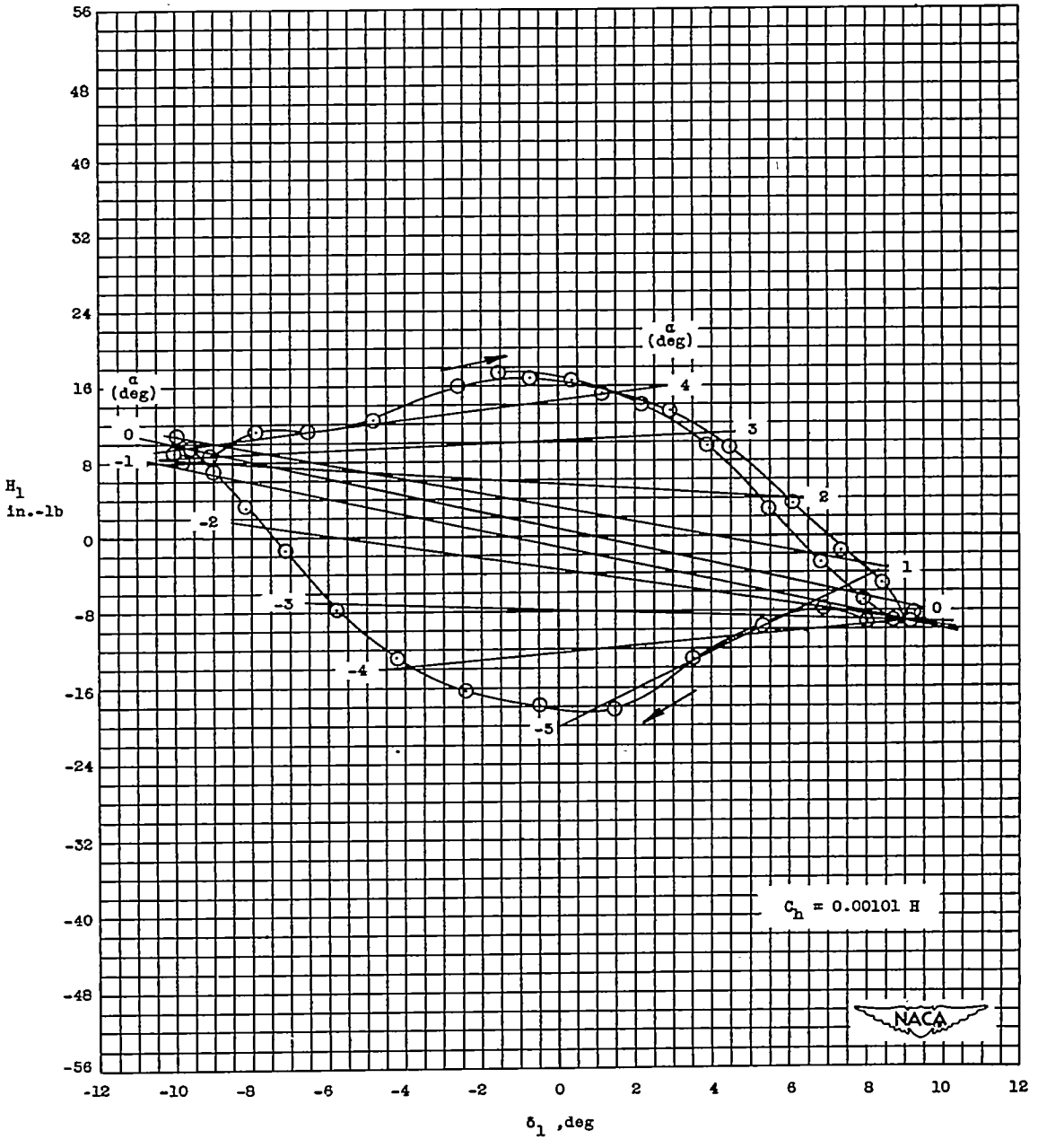

(w) M = 1.30; hinge line at $0.6390c_a$.

Figure 5.- Continued.

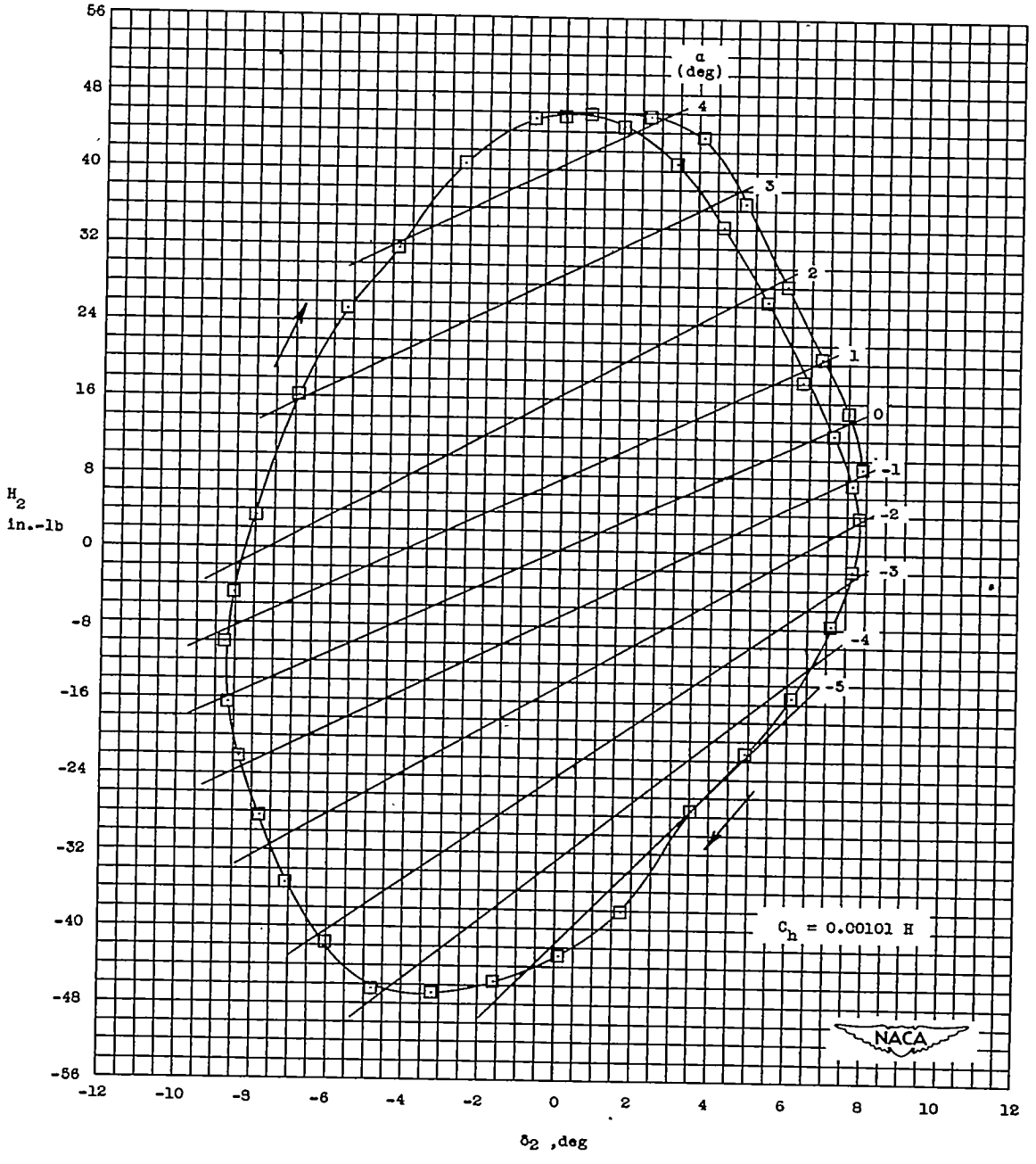

(x) M = 1.30; hinge line at $0.6885c_a$.

Figure 5.- Continued.

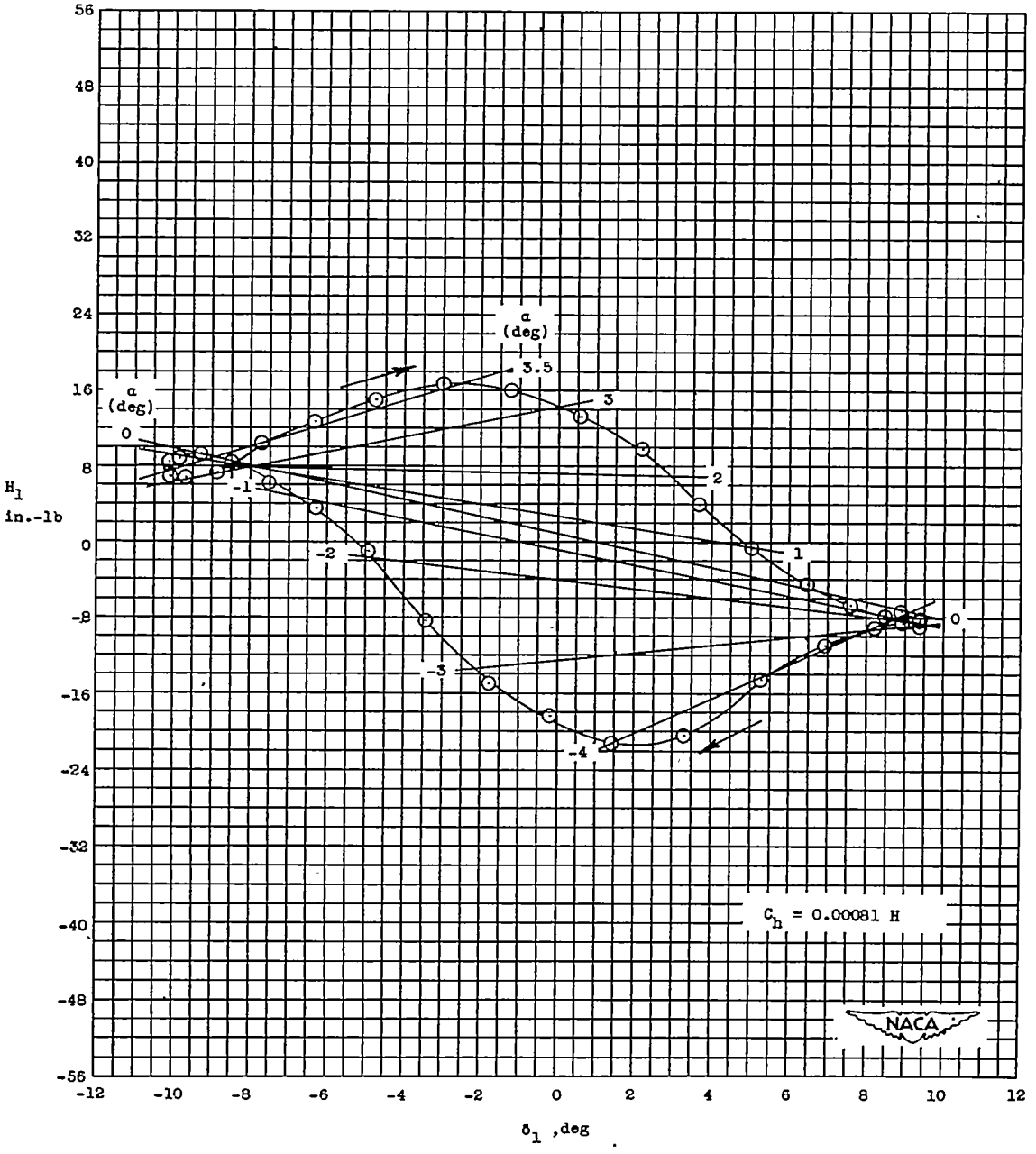

(y) M = 1.43; hinge line at $0.6390c_a$.

Figure 5.- Continued.

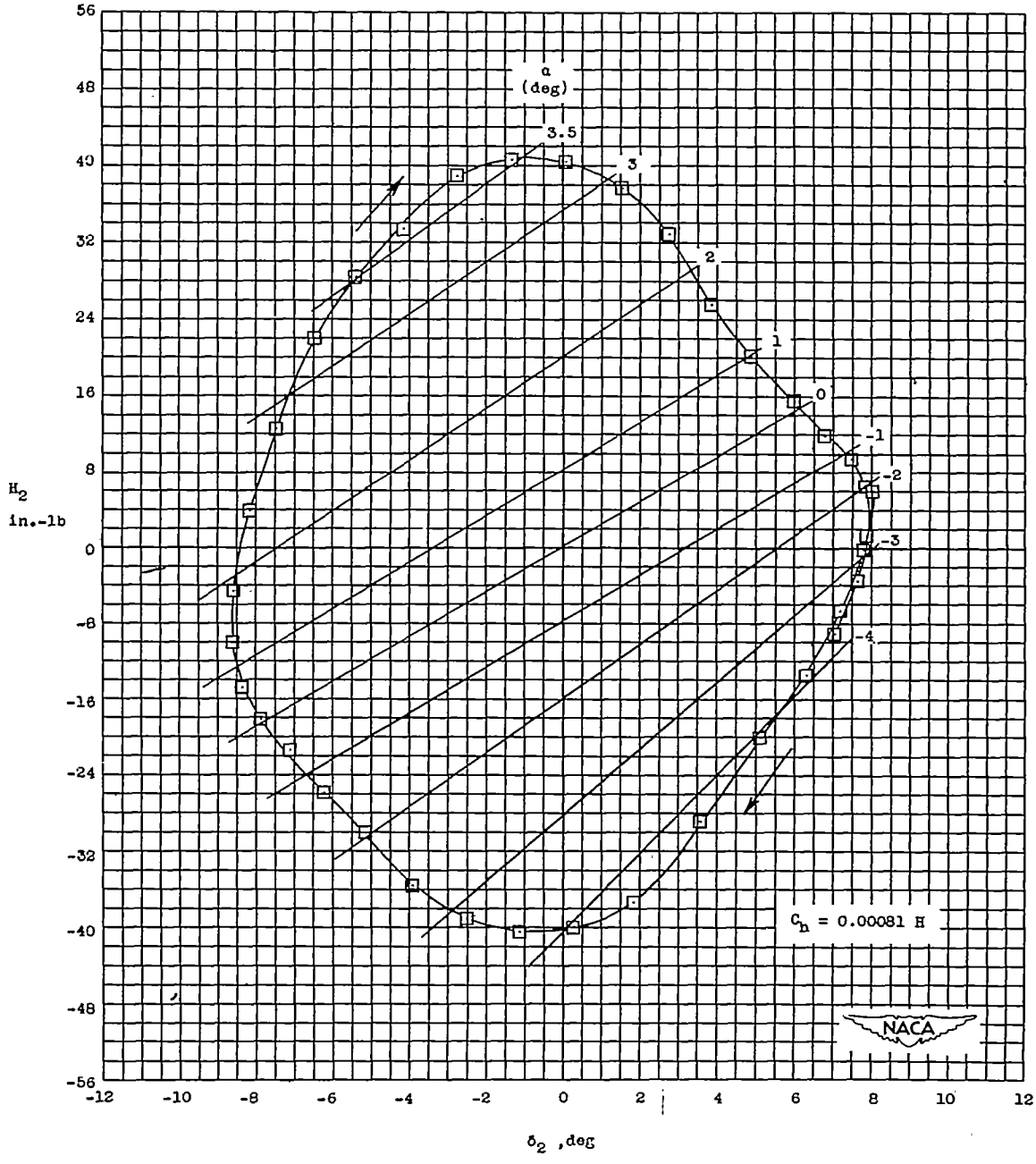

(z) M = 1.43; hinge line at 0.6885c_a.

Figure 5.- Concluded.

[redacted]

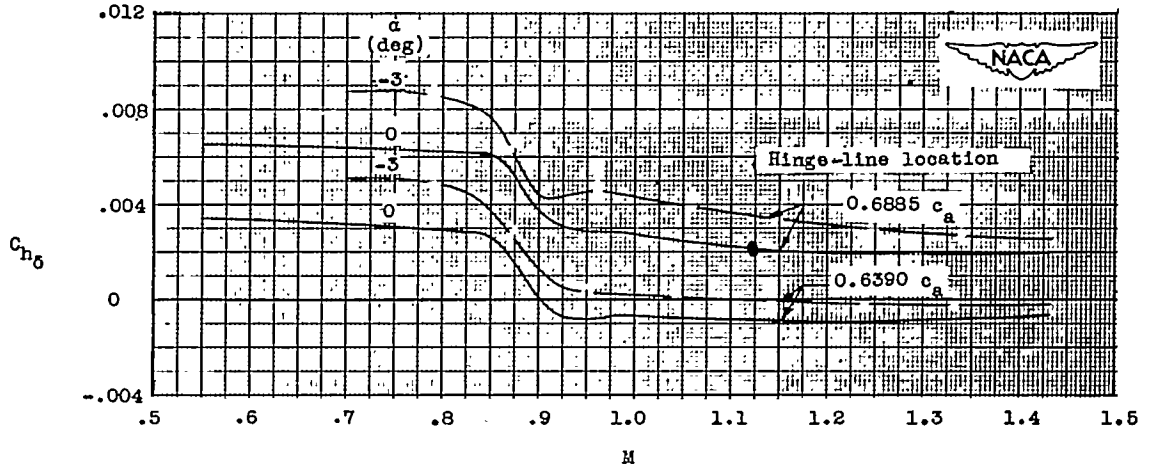

Figure 6.- Variation with Mach number of the change in control-hinge-moment coefficient with respect to control deflection for the two test hinge-line locations.

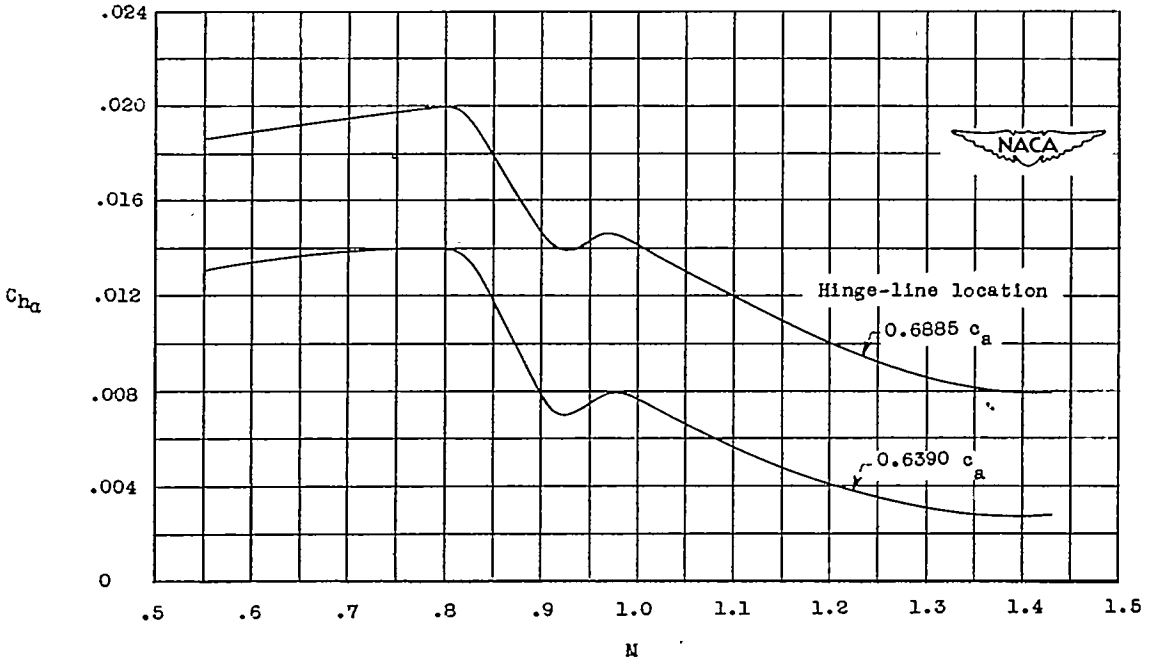

Figure 7.- Variation with Mach number of the change in control-hinge-moment coefficient with respect to angle of attack for the two test hinge-line locations $\delta = 0$.

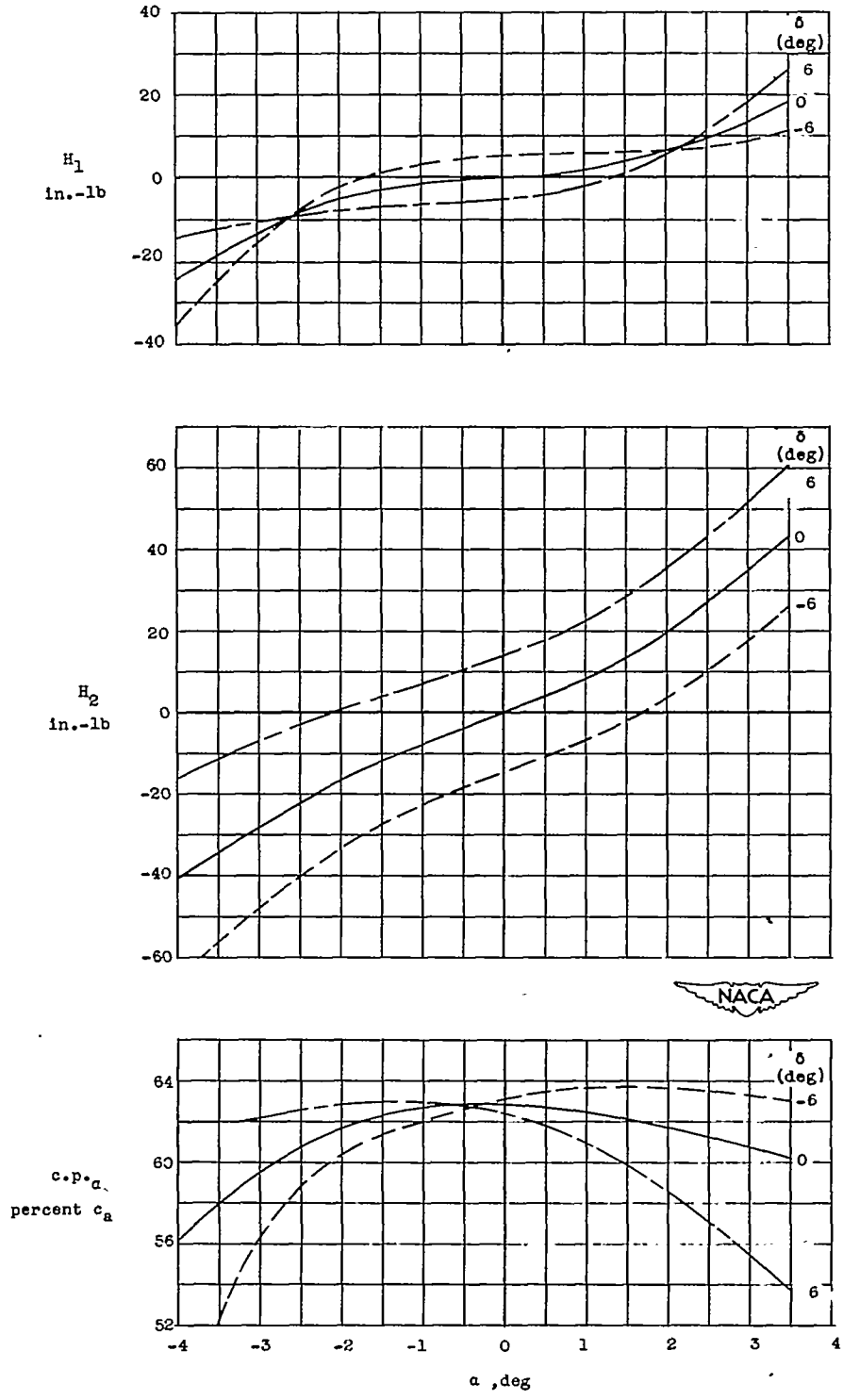

Figure 8.- Variation with angle of attack of hinge moments, for each of the controls, and chordwise location of the center of pressure of the control angle-of-attack loads for deflections of -6°, 0°, and 6°. M = 1.43.

[redacted]

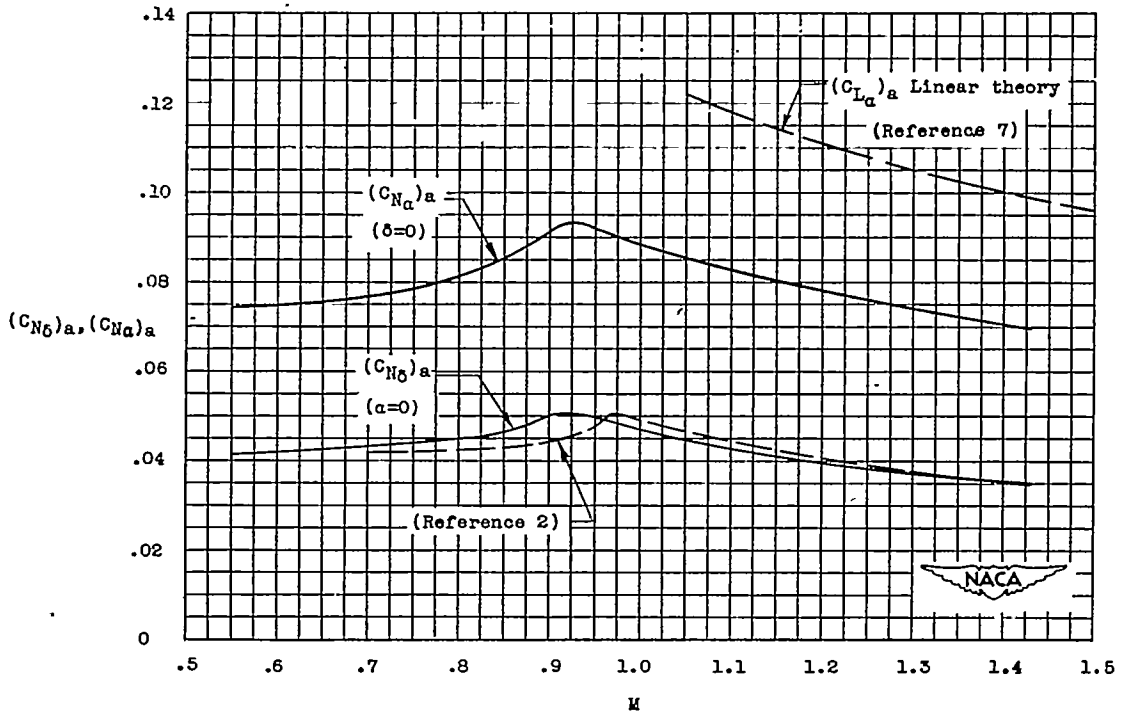

Figure 9.- Variation with Mach number of the change in control-normal-force coefficient with respect to angle of attack and deflection.

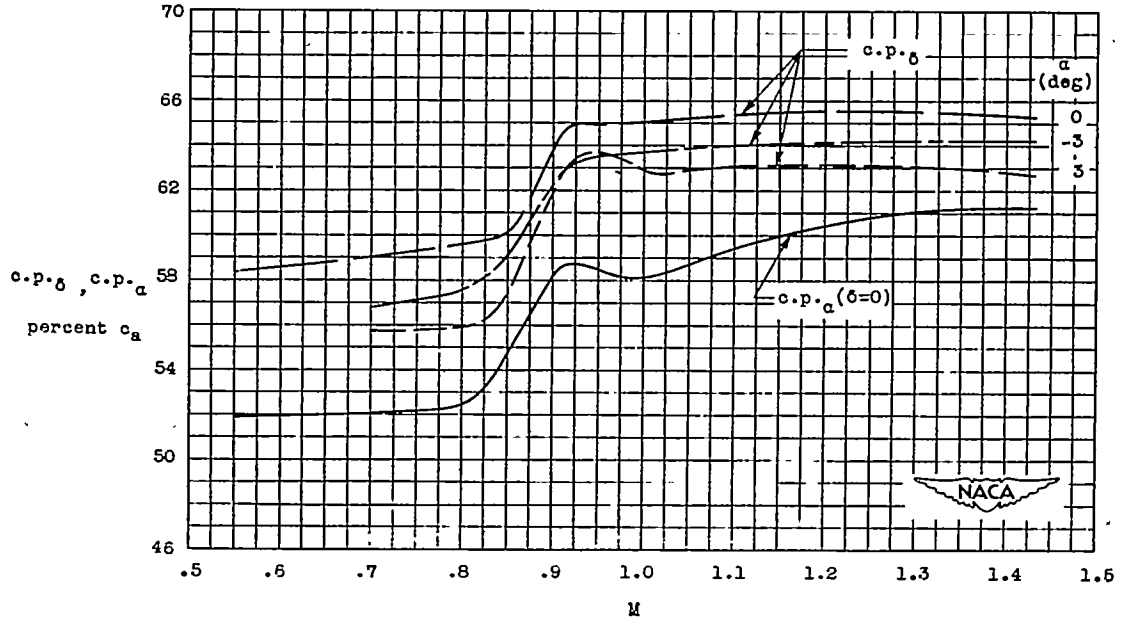

Figure 10.- Mach number variation of the control chordwise center-of-pressure location as evaluated independently for control deflection and angle of attack.

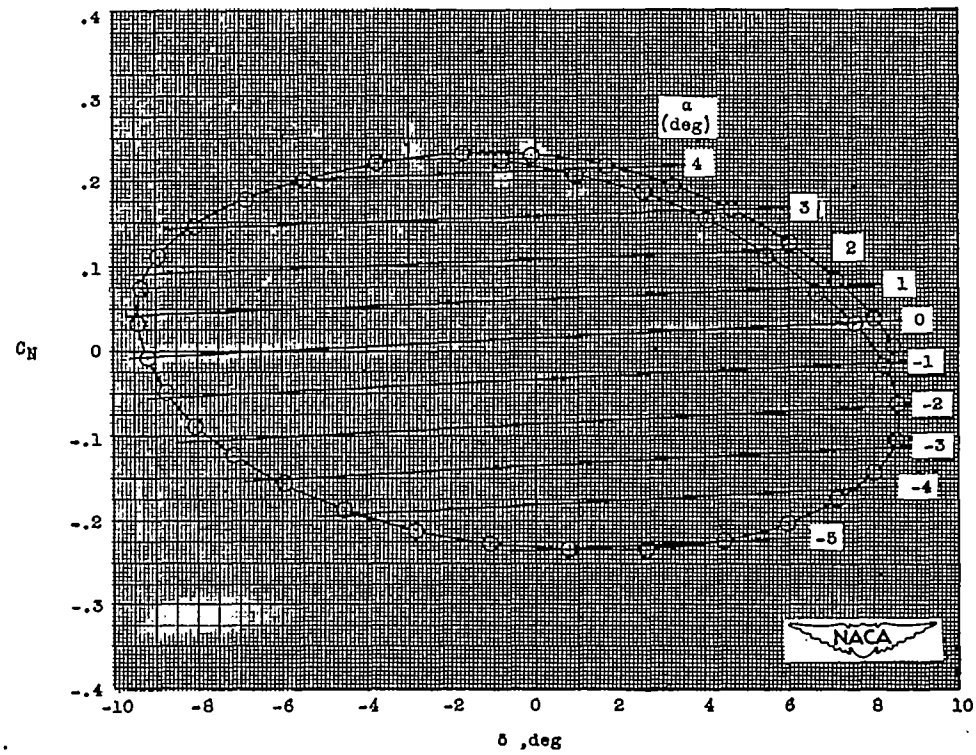

Figure 11.- Variation of normal-force coefficient with control deflection showing lines of constant angle of attack. M = 1.30.

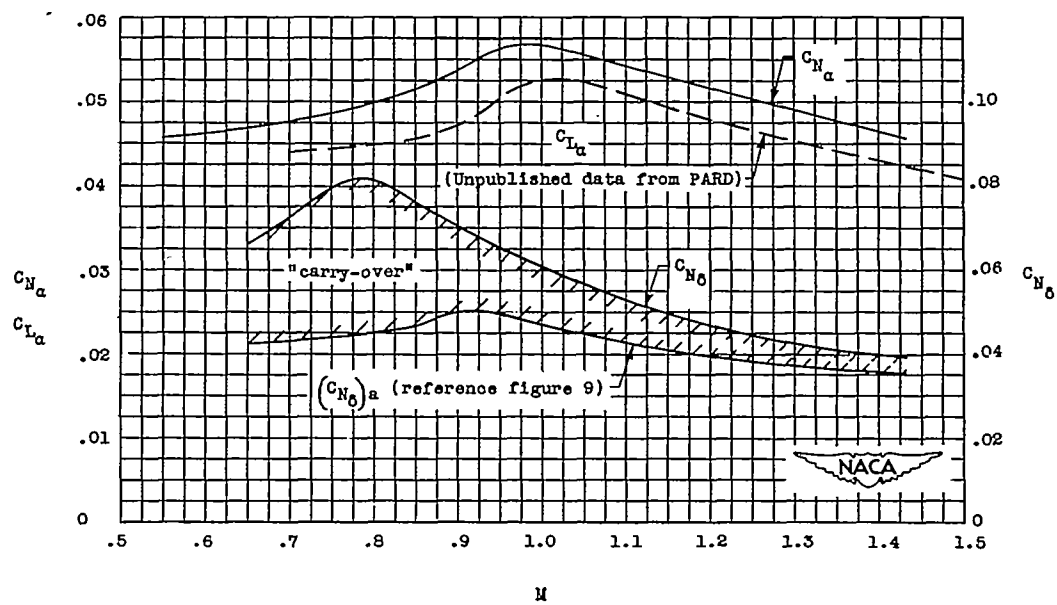

Figure 12.- Variation with Mach number of the model normal-force-coefficient slope with respect to angle of attack and deflection.

NACA-Langley - 10-6-52 - 325